A&A 387, 560–579 (2002)
DOI: 10.1051/0004-6361:20020434

Astronomy & Astrophysics

First stars. I. The extreme r-element rich, iron-poor halo giant CS 31082-001

Implications for the r-process site(s) and radioactive cosmochronology⋆

V. Hill[1], B. Plez[2], R. Cayrel[3], T. C. Beers[4], B. Nordström[5,6], J. Andersen[6], M. Spite[1], F. Spite[1], B. Barbuy[7], P. Bonifacio[8], E. Depagne[1], P. François[3], and F. Primas[9]

[1] Observatoire de Paris-Meudon, GEPI, 2 pl. Jules Janssen, 92195 Meudon Cedex, France
[2] GRAAL, Université de Montpellier II, 34095 Montpellier Cedex 05, France
e-mail: Bertrand.Plez@graal.univ-montp2.fr
[3] Observatoire de Paris, GEPI, 61 av. de l'Observatoire, 75014 Paris, France, e-mail: Roger.Cayrel@obspm.fr
[4] Department of Physics & Astronomy, Michigan State University, East Lansing, MI 48824, USA
[5] Lund Observatory, Box 43, 221 00 Lund, Sweden
[6] Astronomical Observatory, NBIfAFG, Juliane Maries Vej 30, 2100 Copenhagen, Denmark
[7] IAG, Universidade de São Paolo, Departmento de Astronomia, CP 3386, São Paulo, Brazil
[8] Istituto Nazionale per l'Astrofisica – Osservatorio Astronomico di Trieste, via G.B. Tielpolo 11, 34131 Trieste, Italy
[9] European Southern Observatory (ESO), Karl-Schwarschild-Str. 2, 85749 Garching b. München, Germany

Received 28 January 2002 / Accepted 21 March 2002

Abstract. We present a high-resolution ($R = 75\,000$, $S/N \sim 500$) spectroscopic analysis of the bright ($V = 11.7$), extreme halo giant CS 31082-001 ([Fe/H] $= -2.9$), obtained in an ESO-VLT *Large Programme* dedicated to very metal-poor stars. We find CS 31082-001 to be extremely rich in r-process elements, comparable in this respect only to the similarly metal-poor, but carbon-enriched, giant CS 22892-052. As a result of the extreme overabundance of the heaviest r-process elements, and negligible blending from CH and CN molecular lines, a reliable measurement is obtained of the U II line at 386 nm, for the first time in a halo star, along with numerous lines of Th II, as well as lines of 25 other r-process elements. Abundance estimates for a total of 43 elements (44 counting Hydrogen) are reported in CS 31082-001, almost half of the entire periodic table. The main atmospheric parameters of CS 31082-001 are as follows: $T_{\rm eff} = 4825 \pm 50$ K, $\log g = 1.5 \pm 0.3$ (cgs), [Fe/H] $= -2.9 \pm 0.1$ (in LTE), and microturbulence 1.8 ± 0.2 km s^{-1}. Carbon and nitrogen are not significantly enhanced relative to iron. As usual in giant stars, Li is depleted by dilution ($\log$(Li/H) $= 0.85$). The α-elements show the usual enhancements with respect to iron, with [O/Fe] $= 0.6 \pm 0.2$ (from [O I] 6300 Å), [Mg/Fe] $= 0.45 \pm 0.16$, [Si/Fe] $= 0.24 \pm 0.1$, and [Ca/Fe] $= 0.41 \pm 0.08$, while [Al/Fe] is near -0.5. The r-process elements show unusual patterns: among the lightest elements ($Z \sim 40$), Sr and Zr follow the Solar r-element distribution, but Ag is down by 0.8 dex. All elements with $56 \leq Z \leq 72$ follow the Solar r-element pattern, reduced by about 1.25 dex. Accordingly, the [r/Fe] enhancement is about +1.7 dex (a factor of 50), very similar to that of CS 22892-052. Pb, in contrast, seems to be *below* the shifted Solar r-process distribution, possibly indicating an error in the latter, while thorium is more enhanced than the lighter nuclides. In CS 31082-001, $\log$(Th/Eu) is -0.22 ± 0.07, higher than in the Solar System (-0.46) or in CS 22892-052 (-0.66). If CS 31082-001 and CS 22892-052 have similar ages, as expected for two extreme halo stars, this implies that the production ratios were different by about 0.4 dex for the two objects. Conversely, if the Th/Eu production ratio were universal, an age of 15 Gyr for CS 22892-052 would imply a *negative age* for CS 31082-001. Thus, while a universal production ratio for the r-process elements seems to hold in the interval $56 \leq Z \leq 72$, it breaks down in the actinide region. When available, the U/Th is thus preferable to Th/Eu for radioactive dating, for two reasons: (*i*) because of its faster decay rate and smaller sensitivity to observational errors, and (*ii*) because the inital production ratio of the neighboring nuclides ^{238}U and ^{232}Th is more robustly predicted than the ^{151}Eu/^{232}Th ratio. Our current best estimate for the age of CS 31082-001 is 14.0 ± 2.4 Gyr. However, the computed actinide production ratios should be verified by observations of daughter elements such as Pb and Bi in the same star, which are independent of the subsequent history of star formation and nucelosynthesis in the Galaxy.

Key words. Galaxy: evolution – Galaxy: halo – stars: abundances – stars: individual: BPS CS 31082-001 – nuclear reactions, nucleosynthesis, abundances – cosmology: early Universe

Send offprint requests to: V. Hill,
e-mail: Vanessa.Hill@obspm.fr

⋆ Based on observations of program 165.N-0276(A) obtained with the Very Large Telescope of the European Southern Observatory at Paranal, Chile.

1. Introduction

The detailed chemical abundances of the most metal-poor halo stars contain unique information on the earliest

epochs of star formation and nucleosynthesis in our own and other galaxies. Previous studies of these extreme halo stars (Bessell & Norris 1984; Norris et al. 2001; see other references in Table 2 of Cayrel 1996) have revealed abundance patterns that are very unlike those found in the disk and in halo stars with metallicities above [Fe/H] ~ -2.5 (e.g., Pagel & Tautvaišiene 1997), both as regards their systematic trends and the dramatic abundance variations exhibited by some elements. Recently, a few rare stars have been found to exhibit large r-element enhancements, as compared to Solar ratios, suggesting that their observed abundances are dominated by the influence of a single, or at most a very few SNe II progenitors (Sneden et al. 2000a), and opening the way to radioactive dating of these stars, and of the Galaxy, using the "Th/Eu chronometer" (Cowan et al. 1999; Johnson & Bolte 2001).

The difficulty in obtaining the required data for such stars challenges 4m-class telescopes to their limits, hence the accuracy of the results was significantly limited by the resolution and S/N ratio of the available spectra. Therefore, we have conducted a large program at the ESO *Very Large Telescope* (VLT) and its UVES spectrograph to obtain a systematic, homogeneous spectroscopic analysis of a large sample of extreme halo stars from the HK survey of Beers et al. (1992), and ongoing follow-up work. This contribution is the first in a series of several analysis papers to appear from this program.

During this program, the bright ($V = 11.7$), very metal-poor halo giant CS 31082-001, discovered during medium-resolution spectroscopic follow-up of candidate metal-poor stars from the HK survey of Beers and colleagues (Beers et al. 1992; Beers 1999; Beers et al. 2002b) was found to be strongly enhanced in heavy neutron-capture elements. Its large r-element excess, low carbon and nitrogen content (reducing the CN and CH molecular band contamination, see Table 3 and Fig. 1), and our superb VLT/UVES spectra permitted the first ^{238}U abundance measurement in a halo star (Cayrel et al. 2001), as well as a very accurate abundance of ^{232}Th. This discovery opens the way to a new, far more accurate and reliable radioactive chronometer for old stars, based on the ratio U/Th rather than the conventional Th/Eu ratio, provided that the initial production ratio of U/Th can be reliably estimated.

Uranium was first detected outside the Solar System in the spectra of a handful of CP stars (Jaschek & Malaroda 1970; Cowley et al. 1977 and references therein). The huge enhancements of the rare earths and other heavy elements in Ap stars are not fully understood, but radiative support (e.g., Michaud et al. 1976) is generally favoured over a nucleosynthetic origin (Burbidge & Burbidge 1955). Hence, the U abundance in CP stars is not relevant to galactic nucleosynthesis and radioactive chronometry and is not considered further here.

Radioactive age determinations for halo stars have so far relied on the hypothesis that the r-process pattern in such stars matches the Solar pattern, as has been found in the few known r-process-enhanced extreme halo stars CS 22892-052 (Sneden et al. 1996, 2000a) and HD 115444 (Westin et al. 2000). Indeed, it was tentatively concluded that a universal production pattern exists for the r-process elements, independent of the nature of the progenitor star(s) and the detailed history of the subsequent formation of the stars we now observe.

Our first study of the r-process elements in CS 31082-001 (Hill et al. 2001) suggested that significant deviations from the Solar r-process pattern occur in this star. This paper substantiates this result through a detailed abundance study of the star, taking advantage of the very important recent progress in the measurement of the oscillator strengths of the U II 3859.57 Å line (Nilsson et al. 2001a), and the Th II lines (Nilsson et al. 2001b). As a consequence of this new analysis we have revised our measured value of the abundance ratio U/Th in CS 31082-001, and simultaneously reduced its uncertainty, from derived observational errors on the order of 0.15 dex to 0.11 dex. Moreover, new studies of the stellar production of the actinides (Goriely & Arnould 2001) enable a significantly improved discussion of the age determination for CS 31082-001.

This paper is organized as follows: Sect. 2 describes the observations and data reduction, while Sect. 3 presents a detailed analysis of the elements up to nickel. Section 4 presents a re-analysis of the r-process elements, while Sect. 5 addresses the universality or otherwise of the r-process. In Sect. 6 we consider anew the age determination for CS 31082-001. Section 7 summarizes our conclusions.

2. Observations and reductions

CS 31082-001 was first observed at high dispersion ($R > 45\,000$) with the new ESO-VLT spectrograph UVES (Dekker et al. 2000) in August 2000, and was immediately found to display outstandingly strong europium and thorium lines. The star was promptly re-observed at the highest possible resolution ($R = 75\,000$ in the blue arm of the spectrograph) during a subsequent night, and again in October 2000. Most of the spectra were obtained simultaneously in both the blue and red arms of UVES, using a dichroic mirror, as summarized in Table 1.

Reductions were performed using the UVES context within MIDAS. The succession of tasks included bias subtraction from all images, fit and subtraction of the inter-order background from the object and flat-field images, and the averaging of ten flat-fields per night into a master frame. The echelle orders of the object were optimally extracted[1] (assuming a Gaussian profile for the object perpendicular to the dispersion, and a constant for the sky background); the same weights were applied to extract the flat-field, which was then used to correct both for pixel-to-pixel variations and the blaze of the instrument.

[1] In the two frames that were obtained through the image slicer, the extraction was simply an average of all pixels in the object profile, spread over four slices.

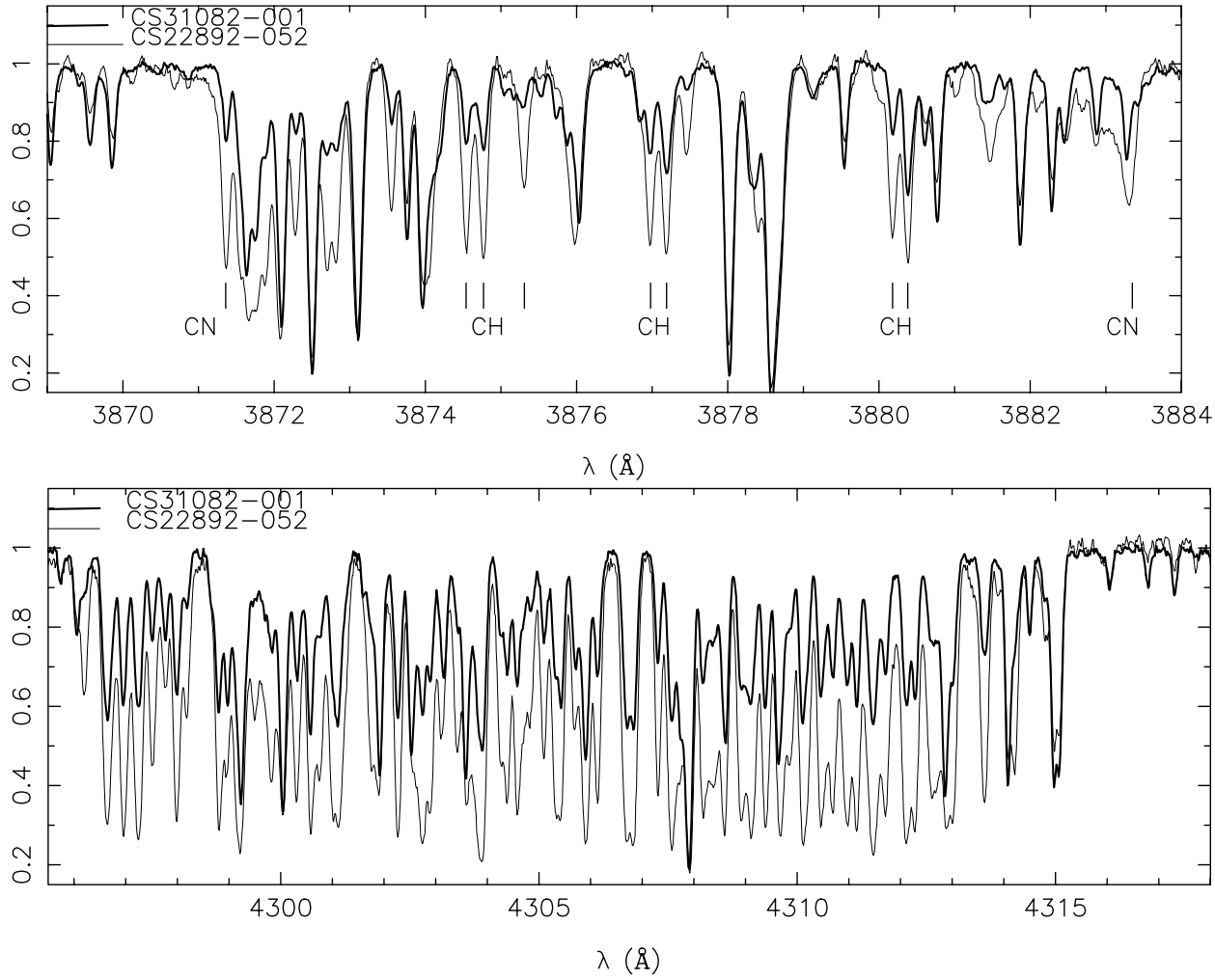

Fig. 1. Comparison of the spectrum of CS 31082-001 (thick line) and CS 22892-052 (narrow line) showing the much reduced molecular band strength in the former. *Upper panel*: CN 3871 and 3883 Å band heads; *lower panel*: G band (CH). The spectrum of CS 22892-052 was obtained during the commissioning of the spectrograph UVES, and is publicly available (`http://www.eso.org/science/uves_comm/`).

Table 1. Log of the observations, and measured signal-to-noise ratio per pixel from the extracted and co-added spectra.

Date	MJD	Exp. time	$\lambda_{\rm start} - \lambda_{\rm end}$	Resolving Power	$\lambda_{\rm start} - \lambda_{\rm end}$	Resolving Power	$V_{\rm r\ barycentric}$
	(s)		Blue		Red		
2000/08/06	51 763.396	1200	335–456 nm	45 000	480–680 nm	45 000	139.03
2000/08/06	51 763.412	1200	335–456 nm	45 000	670–900 nm	45 000	
2000/08/10	51 767.281	3000	335–456 nm*	70 000	–	–	
2000/08/10	51 767.317	3000	335–456 nm*	70 000	–	–	
2000/10/11	51 829.169	7200	310–390 nm	77 000	–	–	
2000/10/14	51 832.176	3600	310–390 nm	77 000	480–680 nm	86 000	139.10
2000/10/14	51 832.219	3600	310–390 nm	77 000	480–680 nm	86 000	139.14
2000/10/15	51 833.223	3600	310–390 nm	77 000	480–680 nm	86 000	139.08
2000/10/17	51 835.147	3600	380–510 nm	75 000	680–1000 nm	86 000	
2000/10/19	51 837.184	3600	380–510 nm	75 000	680–1000 nm	86 000	

*: obtained with Image Slicer

Setting	Total	S/N per pixel						
	Exp. time (s)	@310 nm	@350 nm	@390 nm	@420 nm	@490 nm	@630 nm	@800 nm
310–390 nm	18 000	35	150	350				
335–460 nm	6000		110	250	300			
380–510 nm	7200			250	250	200		
480–680 nm	10 800					250	340	
670–1000 nm	7200							110

The wavelength calibration was performed on Th-Ar lamp frames and applied to the extracted object. The spectra were finally resampled to a constant wavelength step and normalized to unity by fitting a spline function. All spectra obtained with identical spectrograph settings (same cross-disperser and same central wavelength) were then co-added after radial-velocity correction. The lower part of Table 1 summarizes the obtained signal-to-noise ratio per pixel (1 pixel $\sim$ 0.0015 nm) at wavelengths of interest.

Radial velocities given in the table are only those computed from the 480-580nm red spectra (which permitted corrections for small instrumental shifts from the telluric absorption lines). In addition to the spectra reported here, we took exposures of CS 31082-001 with UVES again in September 2001 (5–9 September) and the radial velocity was still impressively unchanged (mean of four measurements in 2001 $V_{\rm r\,barycentric} = 139.05 \pm 0.05$ km s^{-1}) and Aoki (2002, private communication) found $V_{\rm r\,barycentric} = 138.9 \pm 0.24$ km s^{-1} from observations with HDS on the Subaru telescope. There is therefore *no sign* of radial velocity variations in this star, and hence *no hint that CS 31082-001 could be a binary.*

3. Abundance analysis, and derived abundances of the lighter elements

3.1. Model atmosphere and stellar parameters

The adopted model atmospheres (OSMARCS) were computed with the latest version of the MARCS code, initially developed by Gustafsson et al. (1975) and subsequently updated by Plez et al. (1992), Edvardsson et al. (1993), and Asplund et al. (1997). The current version includes up-to-date continuum and line opacities for atomic and molecular species, treated in opacity sampling with more than 10^5 sampling points between 910 Å and 20 μm. Models for CS 31082-001 were computed for a metallicity 1/1000th Solar, with the α-elements boosted by 0.4 dex relative to iron.

In our preliminary analysis of the star (Hill et al. 2001), we were using the synthetic spectrum code of Spite (1967 and subsequent improvements in the last thirty years). In the present analysis we have employed a more consistent approach based on the *turbospec* synthesis code developed by Plez (Plez et al. 1993), which shares routines and input data with OSMARCS. The latest version (Alvarez & Plez 1998) features: Full chemical equilibrium including 92 atomic and over 500 molecular species, Van der Waals collisional broadening by H, He, and H_2 following Anstee & O'Mara (1995), Barklem & O'Mara (1997), and Barklem et al. (1998), and updated continuum opacities, and plane-parallel or spherical geometry. The main differences between the Spite et al. and the Plez codes lie in the continuum opacity, the source function (diffusion is included in the latter), and the collisional broadening calculation.

The effective temperature for the star was computed from multicolor information, using the Alonso et al. (1999) color-temperature transformations. A number of photometric data are available for CS 31082-001: $UBVR_{\rm C}I_{\rm C}$ (subscript C indicating the Cousins system) are from Beers et al. (2002a); the V magnitude and Strömgren photometry are from Twarog et al. (2000); infrared data are available from the DENIS (Fouqué et al. 2000) and 2Mass surveys (Cutri et al. 2000). A summary of these photometric data, and the corresponding derived temperatures, is given in Table 2

Table 2. Colors and effective temperature of CS 31082-001.

Index	value	$T_{\rm eff}$ (K) $E(B-V)$ =0.00	$T_{\rm eff}$ (K) $E(B-V)$ =0.03
V	11.674 ± 0.009		
$(B-V)$	0.772 ± 0.015	4822 ± 120	4903 ± 120
$b-y$	0.542 ± 0.009	4917 ± 70	4980 ± 70
$(V-R)_{\rm C}$	0.471 ± 0.015	4842 ± 150	5027 ± 150
$(V-I)_{\rm C}$	0.957 ± 0.013	4818 ± 125	4987 ± 125
$(V-K)$	2.232 ± 0.008	4851 ± 50	4967 ± 50

At a Galactic latitude $l = -76°$, the observed colors of CS 31082-001 are not expected to be significantly affected by reddening. The Burstein & Heiles (1982) maps suggest negligible reddening; the Schlegel et al. maps (Schlegel et al. 1998) suggest $E(B-V) \approx 0.03$. Table 2 lists effective temperatures derived both for the situation of no reddening, and for an adopted reddening of 0.03 mags. The no-reddening values are in better agreement with the derived excitation temperature from Fe I lines. The final adopted temperature of $T_{\rm eff} = 4825$ K is consistent with that obtained from the excitation equilibrium of the Fe I lines. A gravity of $\log g = 1.5 \pm 0.3$ dex was assumed in order to satisfy the ionization equilibrium of iron and titanium, and a microturbulence velocity of $\xi = 1.8 \pm 0.2$ km s^{-1} was obtained from the requirement that strong and weak lines of iron yield the same abundance.

In this paper we are mostly concerned with the relative abundances of elements in this star, especially the abundance pattern of the heavy neutron-capture elements. The relative abundances are only very weakly dependent on the adopted stellar parameters; all of the lines of interest respond similarly to small changes in temperature and gravity, hence the pattern of the heavy elements relative to one another is hardly affected. A thorough discussion of errors is provided in Sect. 4.2.

3.2. Abundances of light and iron-peak elements

Most of the abundances for the light and the iron-group elements were determined via equivalent width measurement of a selection of unblended lines. Exceptions are Li, C, N, and O, for which synthesis spectra were directly compared to the observed spectrum. The linelist used for

Table 3. LTE abundances for lighter elements in CS 31082-001.

El.	Z	$\log\epsilon$	[X/H]	σ	$N_{\rm lines}$	[X/Fe]	Δ[X/Fe]
^{12}C/^{13}C		>20					
Li I	3	0.85			1		0.11
C	6	5.82	−2.7	0.05		+0.2	
N	7	<5.22	<−2.7			<+0.2	
O I	8	6.52	−2.31		1	0.59	0.20
Na I	11	3.70	−2.63	0.02	2	0.27	0.13
Mg I	12	5.04	−2.54	0.13	7	0.36	0.16
Al I	13	2.83	−3.64		1	−0.74	0.17
Si I	14	4.89	−2.66		1	0.24	0.10
K I	19	2.87	−2.25	0.08	2	0.65	0.10
Ca I	20	3.87	−2.49	0.11	15	0.41	0.08
Sc II	21	0.28	−2.89	0.07	7	0.01	0.06
Ti I	22	2.37	−2.65	0.09	14	0.25	0.10
Ti II	22	2.43	−2.59	0.14	28	0.31	0.05
Cr I	24	2.43	−3.24	0.11	7	−0.34	0.11
Mn I	25	2.14	−3.25	0.09	6	−0.35	0.10
Fe I	26	4.60	−2.90	0.13	120	0.00	
Fe II	26	4.58	−2.92	0.11	18	0.02	
Co I	27	2.28	−2.64	0.11	4	0.26	0.12
Ni I	28	3.37	−2.88	0.02	3	0.02	0.14
Zn I	30	1.88	−2.72	0.00	2	0.18	0.09

all light and iron-peak elements will be published together with the analysis of the complete sample of our Large Program. For the compilation of this linelist, we used the VALD2 compilation of Kupka et al. (1999).

Table 3 lists the mean abundances[2], dispersion of the single line measurements around the mean (σ), and the number of lines used to determine the mean abundances of all measured elements from lithium to zinc. Also listed are the abundances relative to iron, [X/Fe], and the total uncertainty on this ratio, Δ[X/Fe], including errors linked both to observations and the choice of stellar parameters (similarly to the Δ[X/Th] reported in Table 6 and explained in Sect. 4.2). Notes on specific elements are:

Lithium

With an equivalent width of more than 15 mÅ, the lithium 6708 Å line is easily detected in this star. The abundance was determined using spectrum synthesis techniques to account for the doublet nature of the line. With an abundance of $\log\epsilon$(Li) = 0.85, CS 31082-001 falls well below the lithium plateau for hot dwarf halo stars, as expected for a red giant. However, not all lithium in this star has been diluted after the first dredge-up, as observed in many metal-poor giants. In fact, in a sample of 19 giants with [Fe/H] ≤ -2.7 (Depagne et al. 2002), we find that among the eight giants with gravities close to $\log g = 1.5$, four have detectable lithium. Hence, in this respect, CS 31082-001 is not exceptional.

[2] In the classical notation where $\log\epsilon(\mathrm{H}) = 12$ and $[\mathrm{X/H}] = \log(N_{\rm X}/N_{\rm H})_* - \log(N_{\rm X}/N_{\rm H})_\odot$.

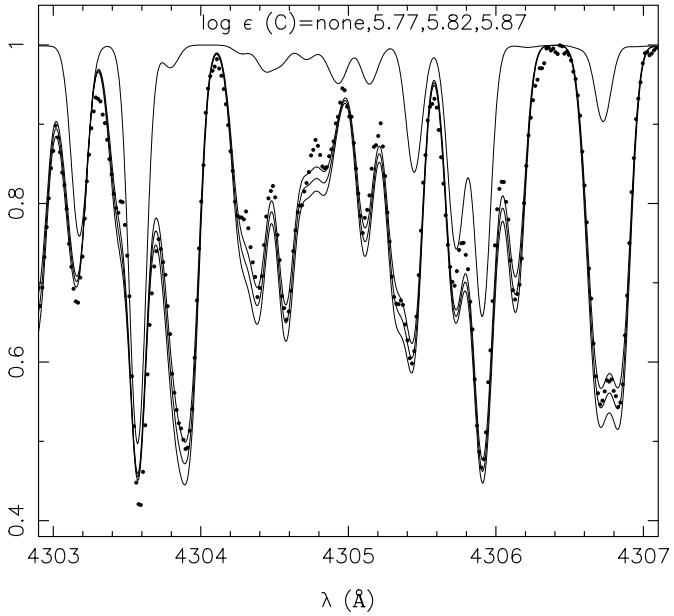

Fig. 2. Fit of CH lines of the G band in CS 31082-001. *Dots*: observations, *lines*: synthetic spectra computed for the abundances indicated in the figure.

Carbon and nitrogen

These two elements are detected via the molecular bands of CH and CN. Line lists for ^{12}CH, ^{13}CH, ^{12}C^{14}N, and ^{13}C^{14}N were included in the synthesis. The CN linelists were prepared in a similar fashion as the TiO linelist of Plez (1998), using data from Cerny et al. (1978), Kotlar et al. (1980), Larsson et al. (1983), Bauschlicher et al. (1988), Ito et al. (1988), Prasad & Bernath (1992), Prasad et al. (1992), and Rehfuss et al. (1992). Programs by Kotlar were used to compute wavenumbers of transitions in the red bands studied by Kotlar et al. (1980). For CH, the LIFBASE program of Luque & Crosley (1999) was used to compute line positions and *gf*-values. Excitation energies and isotopic shifts (LIFBASE provides only line positions for ^{12}CH) were taken from the line list of Jørgensen et al. (1996). By following this procedure, a good fit of CH lines could be obtained, with the exception of a very few lines which we removed from the list.

^{13}C isotopic lines could not be detected, hence we only provide a lower limit on the ^{12}C/^{13}C ratio, based on the non-detection of ^{13}CH lines.

The carbon abundance was derived primarily from CH lines in the region 4290–4310 Å (the CH A–X 0–0 bandhead), which is almost free from intervening atomic lines. We derive an abundance $\log\epsilon(\mathrm{C}) = 5.82 \pm 0.05$ (see

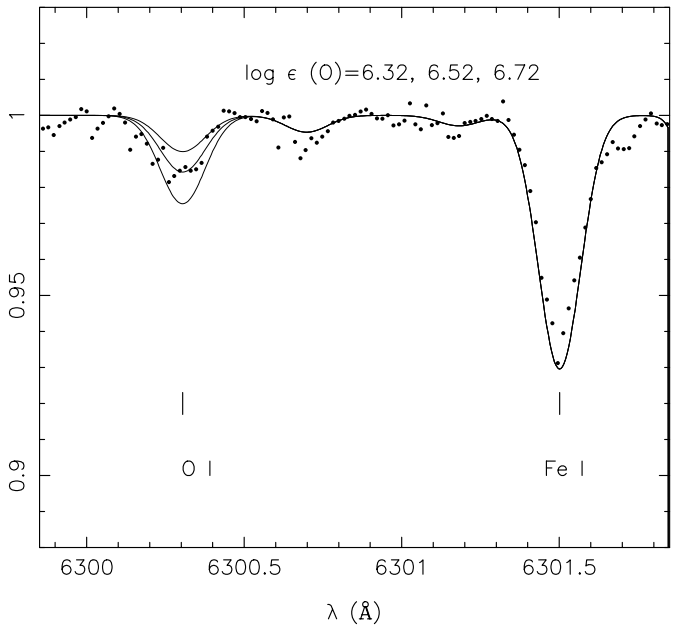

Fig. 3. The forbidden [O I] 6300 Å line in CS 31082-001. Symbols as in Fig. 2.

Fig. 2). With this same abundance, a good fit is obtained in the more crowded regions around 3900 Å and 3150 Å, where the B–X and C–X bandheads occur.

The nitrogen abundance was then derived from CN lines. It was only possible to set an upper limit, since the CN lines are extremely weak. A conservative estimate of the nitrogen abundance is $\log\epsilon(N) = 5.22$, from the 3875–3900 Å B–X 0–0 bandhead. An attempt was also made to use the NH 0–0 bandhead of the A–X system around 3350 Å. Lines were extracted from the Kurucz line database (1993), and the gf-values were scaled with the mean correction derived by comparison of the Kurucz and Meyer & Roth (1991) gf-values for the 2 (0–0) $R_1(0)$ and ${}^RQ_{21}(0)$ lines at 3358.0525 Å and 3353.9235 Å. This derived correction, -0.807 in $\log(gf)$, was applied to all of the NH lines. The fit was poor, but if the gf-values are correct, which is a bold assumption, the nitrogen abundance is at most $\log\epsilon(N) = 5.02$. Given the many uncertainties attached to this latter determination, we adopt the more conservative estimate obtained from CN.

Oxygen

The forbidden oxygen line at 630 nm is clearly detected in the three spectra taken in October 2000, where the motion of the Earth relative to the star resulted in a Doppler shift that moved this weak line clear of the neighboring telluric absorption lines (Fig. 3). The measured equivalent width of the [OI] line is 2.7 mÅ; the corresponding abundance is $\log\epsilon(\mathrm{O}) = 6.52$, which in turn implies an overabundance of oxygen with respect to iron of $[\mathrm{O/Fe}] = +0.59 \pm 0.2$.

Thus, CS 31082-001 has an oxygen abundance that is consistent with the mild oxygen enhancement observed for other halo stars, at least when derived from the same forbidden [OI] line (e.g. Barbuy et al. 1988; Sneden et al. 2001; Nissen et al. 2001). The linearly increasing trend of [O/Fe] with decreasing metallicity suggested from measurements of OH lines in the UV of halo turnoff stars (e.g., Israelian et al. 1998; Boesgaard et al. 1998) is not a relevant comparison here, since it is known that there exist systematic differences between the two indicators (UV OH and [OI]), that could arise, for example, from temperature inhomogeneity effects (see Asplund & García Pérez 2001).

All of the α-elements in CS 31082-001 are enhanced by 0.35 to 0.6 dex relative to iron ($[\alpha/\mathrm{Fe}] = +0.37 \pm 0.13$, where α is the mean of O, Mg, Si, Ca, and Ti), consistent with the observed behavior of other metal-poor halo stars.

Potassium is also observed in CS 31082-001, from the red lines at 7664 Å and 7698 Å; an LTE analysis yields $[\mathrm{K/Fe}]_{\mathrm{LTE}} = +0.65$. However, Ivanova & Shimanskii (2000) have shown that these transitions suffer from significant NLTE effects. For a star with $T_{\mathrm{eff}} = 4800$ K, $\log g = 1.5$, the correction amounts to ~ -0.33 dex. Therefore, the true potassium abundance in CS 31082-001 should be around $[\mathrm{K/Fe}] = +0.3$ dex.

Iron group (Cr through Ni)

Among the elements of this group, all are depleted to a similar level as iron, although Co is up by ∼0.3 dex, while Cr and Mn are down by ∼0.3 dex, a typical behaviour for metal-poor stars (e.g., McWilliam et al. 1995; Ryan et al. 1996). Thus, both in this respect, and from its standard $[\alpha/\mathrm{Fe}]$ enhancement, CS 31082-001 appears to be a typical very metal-poor halo star, except for its high neutron-capture-element abundances. This behavior is understandable if the light elements are produced in the hydrostatic burning phase of the evolution of massive stars, whereas the r-process elements are produced during the explosive synthesis phase of the SNe.

Zinc

Zinc is present in CS 31082-001 at a level comparable to the iron-group elements, and thus does not share the strong enhancement of neutron-capture elements in this star. This is relevant to the ongoing discussions on the origin of Zn in halo stars (Umeda & Nomoto 2002 and references therein), and the importance of the neutron-capture channel for Zn production. Either Zn does not arise from neutron-capture processes, or these processes are unimportant in r-process conditions.

4. Neutron-capture elements

In this section we discuss our adopted linelist, and examine the possible sources of error affecting the abundance determination of neutron-capture elements. We then explore the abundance patterns of elements in the three r-process peaks. Eight elements with atomic numbers $38 \leq Z \leq 47$ were measured in the region of the first peak. The second peak is the best constrained, with thirteen elements measured in the range $56 \leq Z \leq 72$. The third peak and the actinides are probed by four elements with measured abundances in the region $76 \leq Z \leq 92$.

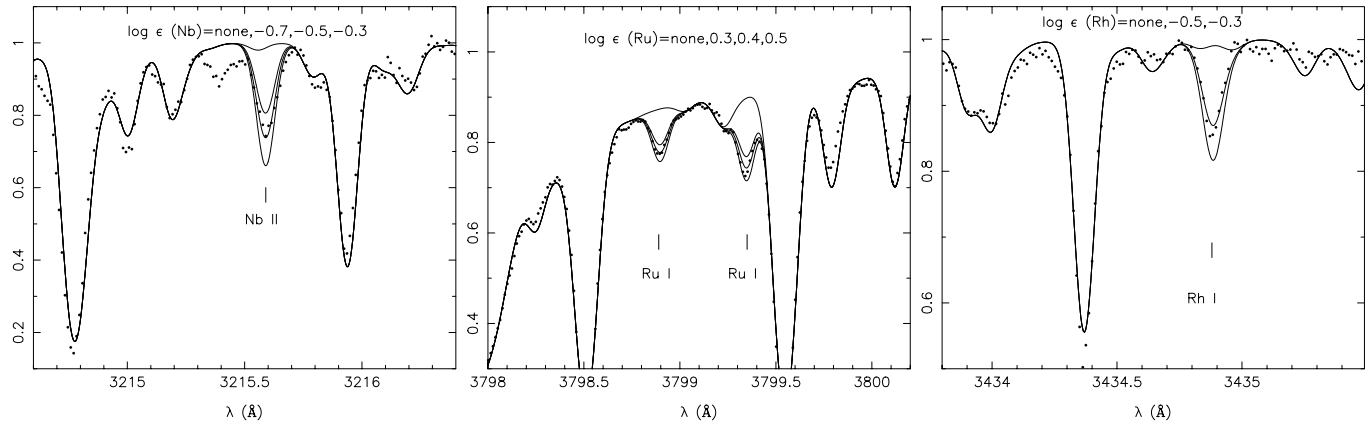

Fig. 4. The observed Nb II 3215 Å, Ru I 3799 Å, and Rh I 3434 Å lines in CS 31082-001. Symbols as in Fig. 2.

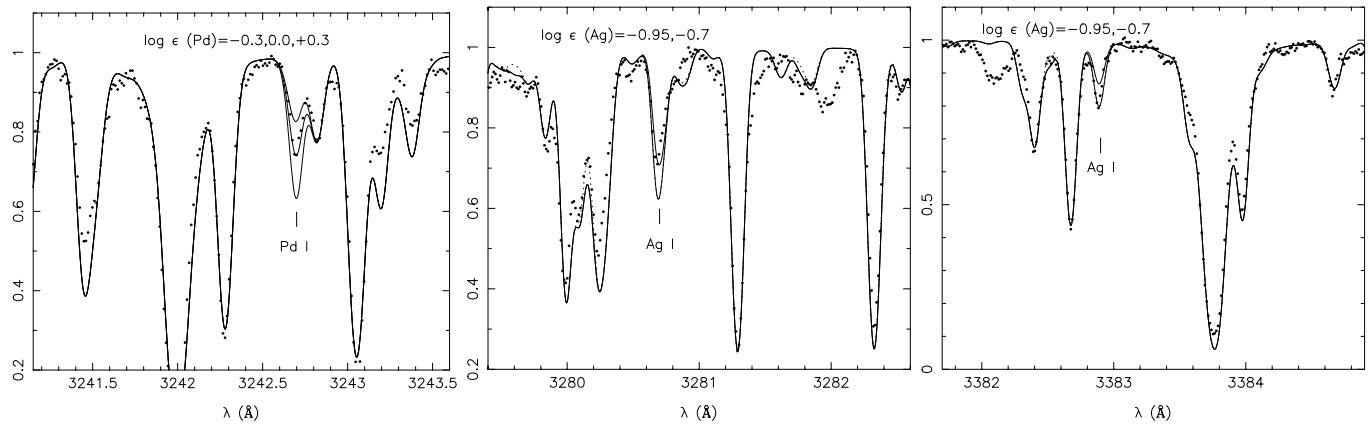

Fig. 5. The observed Pd I 3242 Å, Ag I 3281 Å, and 3383 Å lines in CS 31082-001. Symbols as in Fig. 2.

4.1. Linelists and physical data

Lines from 28 neutron-capture elements were observed in CS 31082-001, mainly concentrated in the blue and UV parts of the spectrum. The full linelist for heavy elements is provided in an Appendix to this paper, which also lists the references for our adopted oscillator strengths. When available from the paper of Sneden et al. (1996), the same oscillator strengths were adopted in order to make the comparison to the star CS 22892-052 easier. However, more lines were measured here, hence we had to supplement this compilation with additional information. In particular, we note that new results on the lifetimes and branching factors of both uranium (Nilsson et al. 2001a) and thorium (Nilsson et al. 2001b) transitions are now available; we make use of them here (Table 4). The Appendix also lists equivalent widths of the lines in CS 31082-001 and the individual derived abundances. In cases when blending was severe, or hyperfine structure was important, abundances were determined by comparing the observations directly to synthetic spectra (in these cases, no equivalent widths are listed in the Appendix). Hyperfine structure was included for the Ba and Eu lines. The mean abundances obtained for each element are listed in Table 5. Figures 4 to 10 are representative examples of the quality of the observed spectrum, and the fits to synthetic spectra.

Table 4. Th and U lines used in the abundance determination.

λ(Å)	$\chi_{\rm ex}$(eV)	$\log gf$	$\log\epsilon$
Th II			
3351.229	0.188	−0.600	−0.88
3433.999	0.230	−0.537	−0.80
3435.977	0.000	−0.670	−0.85
3469.921	0.514	−0.129	−0.93
3675.567	0.188	−0.840	−0.83
4019.129	0.000	−0.228	−1.04
4086.521	0.000	−0.929	−0.96
4094.747	0.000	−0.885	−1.05
U II			
3859.571	0.036	−0.067	−1.92

4.2. Error budget

Table 6 summarizes the various sources of uncertainties affecting the derived neutron-capture-element abundances in CS 31082-001. Stochastic errors (Δ(obs) listed in Col. 6) arise from random uncertainties in the

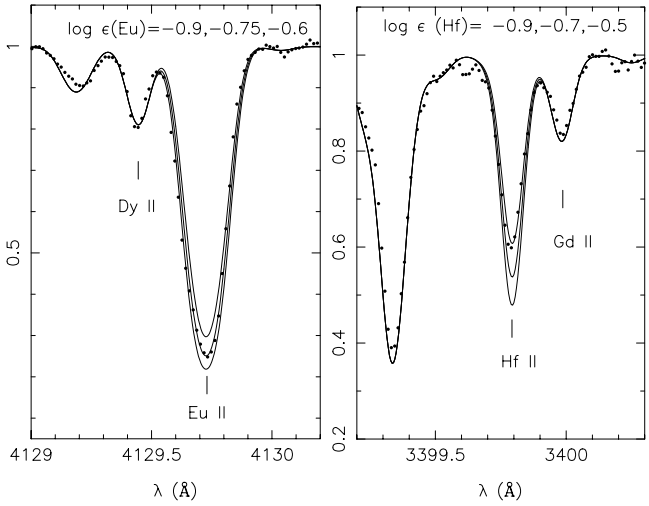

Fig. 6. The observed Eu 4129 and Hf II 3999 Å line in CS 31082-001. Symbols as in Fig. 2.

oscillator strengths (*gf* values) and in the measured equivalent widths. The magnitude of this error is estimated as $\sigma/\sqrt{N-1}$ (where σ is the rms around the mean abundance) when $N \geq 2$ lines of a given element are observed, otherwise as the quadratic sum of the estimated error on the adopted *gf* value and the fitting uncertainty. Systematic uncertainties include those which exist in the adopted oscillator strengths, in the equivalent width measurements, mostly related to continuum location, and in the adopted stellar parameters. The first is extremely difficult to assess and is not considered explicitly here, although it might be significant (*gf* values from various sources may be cross-checked, but often only one source is available). The second should be negligible, given the very high quality of our data. Hence we have examined here only those errors linked to our choice of stellar parameters. These were estimated by varying $T_{\rm eff}$ by +100 K, $\log g$ by +0.3 dex, and ξ by +0.2 km s^{-1} in the stellar atmosphere model (Cols. 2, 3, and 4, respectively). The quantity $\Delta(T,\ \log g,\ \xi)$ listed in Col. 5 is the total impact of varying each of the three parameters, computed as the quadratic sum of Cols. 2, 3, and 4. The total uncertainty Δ(total) (Col. 7) on the *absolute* abundance of each element ($\log \epsilon$(X)) is computed as the quadratic sum of the stochastic and systematic errors. Columns 8 and 9 list the total uncertainties on the abundance ratios X/U and X/Th. Note that, due to the similarity of the response of a given set of elements to changes in the stellar parameters, systematic errors largely cancel out in the measured *ratios* of these elements, reducing the uncertainty affecting the *relative* abundances. However, for the few species that are determined from neutral lines, the stellar parameters uncertainties impact on the [X/Th] or [X/U] ratio is not negligible anymore (e.g. Ru, Rh, Pd).

In the following discussion, since we are mostly concerned by the *relative* abundance ratios, we chose to consider the total uncertainties on the X/Th ratio as representative of the uncertainty on the abundance pattern (in Figs. 11 and 12, and listed in column $\Delta \log \epsilon$(X/Th) of Table 5).

Table 5. Neutron-capture-element abundances in CS 31082-001.

El.	Z	$\log \epsilon$(X)	σ	$\Delta \log \epsilon$ (X/Th)	$N_{\rm lines}$	[X/Fe]
Sr	38	0.72	0.03	0.08	3	+0.65
Y	39	−0.23	0.07	0.06	9	+0.43
Zr	40	0.43	0.15	0.09	5	+0.73
Nb	41	−0.55		0.15	1	+0.93
Ru	44	0.36	0.10	0.14	5	+1.42
Rh	45	−0.42	0.03	0.13	3	+1.36
Pd	46	−0.05	0.10	0.15	3	+1.16
Ag	47	−0.81	0.17	0.22	2	+1.15
Ba	56	0.40	0.17	0.11	6	+1.17
La	57	−0.60	0.04	0.06	5	+1.13
Ce	58	−0.31	0.10	0.04	9	+1.01
Pr	59	−0.86	0.12	0.06	6	+1.33
Nd	60	−0.13	0.17	0.05	18	+1.27
Sm	62	−0.51	0.16	0.06	9	+1.38
Eu	63	−0.76	0.11	0.05	9	+1.63
Gd	64	−0.27	0.15	0.06	9	+1.51
Tb	65	−1.26	0.07	0.04	7	+1.74
Dy	66	−0.21	0.13	0.07	6	+1.55
Er	68	−0.27	0.08	0.09	5	+1.70
Tm	69	−1.24	0.10	0.08	4	+1.66
Hf	72	−0.59		0.17	2	+1.43
Os	76	0.43	0.17	0.16	3	+1.30
Ir	77	0.20		0.11	2	+1.75
Pb	82	<−0.2:			1	
Th	90	−0.98	0.05	0.11	8	+1.83
U	92	−1.92		0.11	1	+1.49

4.3. The lighter elements, $38 \leq Z \leq 48$

This group includes the classically observed elements Sr, Y, and Zr, but also the less well-studied species Nb, Ru, Rh, Pd, and Ag, whose lines are weak and lie in the near-UV part of the spectrum, hampering their detection in normal metal-poor halo giants. The only metal-poor star in which all these elements have been previously detected is CS 22892-052 (Sneden et al. 2000a), thanks to its large enhancement of neutron-capture elements. In CS 31082-001 we detected even more lines of these elements (due to the slightly larger metallicity, reduced blending by CH, CN and NH molecules, and better spectrum quality); Figs. 4 and 5 show examples of the quality of the fits obtained. However, one element detection remains inconclusive – even the strongest expected transition of Cd I in our wavelength domain (3261.05 Å) is too severely blended to be useful for abundance determinations.

Table 6. Error budget for neutron-capture elements.

El.	ΔT	$\Delta \log g$	$\Delta\xi$	$\Delta(T, \log g, \xi)$	Δ(obs)	Δ(total)	$\Delta \log \epsilon$(X/U)	$\Delta \log \epsilon$(X/Th)
	+100 K	+0.3 dex	+0.2 km s^{-1}					
(1)	(2)	(3)	(4)	(5)	(6)	(7)	(8)	(9)
Sr II	0.064	0.045	−0.047	0.092	0.030	0.10	0.13	0.08
Y II	0.068	0.082	−0.057	0.121	0.023	0.12	0.13	0.06
Zr II	0.066	0.087	−0.034	0.114	0.075	0.14	0.14	0.09
Nb II	0.044	0.091	−0.019	0.128	0.150	0.20	0.19	0.15
Ru I	0.079	−0.021	−0.012	0.159	0.050	0.17	0.18	0.14
Rh I	0.080	−0.019	−0.007	0.162	0.021	0.16	0.17	0.13
Pd I	0.081	−0.023	−0.024	0.166	0.071	0.18	0.19	0.15
Ag I	0.081	−0.022	−0.020	0.166	0.170	0.24	0.24	0.22
Ba II	0.096	0.046	−0.075	0.122	0.076	0.14	0.16	0.11
La II	0.080	0.083	−0.056	0.128	0.020	0.13	0.12	0.06
Ce II	0.078	0.089	−0.013	0.119	0.035	0.12	0.12	0.04
Pr II	0.078	0.089	−0.012	0.119	0.054	0.13	0.12	0.06
Nd II	0.078	0.086	−0.024	0.119	0.041	0.13	0.12	0.05
Sm II	0.082	0.089	−0.010	0.122	0.057	0.13	0.12	0.06
Eu II	0.078	0.090	−0.014	0.120	0.039	0.13	0.12	0.05
Gd II	0.074	0.088	−0.032	0.120	0.053	0.13	0.13	0.06
Tb II	0.078	0.091	−0.016	0.121	0.029	0.12	0.11	0.04
Dy II	0.076	0.088	−0.023	0.118	0.058	0.13	0.13	0.07
Er II	0.078	0.080	−0.088	0.142	0.040	0.15	0.15	0.09
Tm II	0.092	0.053	−0.043	0.115	0.058	0.13	0.14	0.08
Hf II	0.042	0.086	−0.028	0.123	0.170	0.21	0.20	0.17
Os I	0.078	0.011	−0.008	0.157	0.120	0.20	0.19	0.16
Ir I	0.065	0.045	−0.024	0.140	0.090	0.17	0.15	0.11
Th II	0.048	0.090	−0.008	0.132	0.020	0.13	0.11	...
U II	0.046	0.093	−0.002	0.131	0.110	0.17	...	0.11

In Solar System material, the four lighter elements are dominated by products of the main s-process (with a possible contribution from the weak s-process as well; see Prantzos et al. 1990; Tsujimoto et al. 2000), while the elements Ru, Rh, Pd, and Ag may contain a large r-process fraction (54% to 86%). However, in a star as metal-poor as CS 31082-001, it is expected that the s-process contribution should be negligible, both from a theoretical point of view (the main s-process takes place in AGBs, where the contribution depends on metallicity via the abundances of both seed nuclei and neutron sources, e.g. Prantzos et al. 1990), and from an observational point of view (Burris et al. 2000 and references therein). Thus, all these elements should represent r-process material produced in the early Galaxy.

In Fig. 11 we compare the observed abundance pattern in CS 31082-001 to the Solar System r-process abundances, scaled to the abundance of CS 31082-001 (see Sect. 4.4 for details of the scaling procedure). These Solar System r-process abundances are obtained from a decomposition of the Solar abundances (Anders & Grevesse 1989) into their s- and r-process fractions, by subtraction of computed main s-process yields (AGB yields) from the total abundances to obtain the r-process fraction. We show here two sources for this de-composition, illustrating the uncertainties involved. The dashed line in Fig. 11 follows the compilation of Burris et al. (2000), which uses yields from Käppeler et al. (1989) and Wisshak et al. (1996), while the solid line uses yields of AGB models from Arlandini et al. (1999).

It is clear from inspection of Fig. 11 that, although one can argue the case for general agreement in the region of the second r-process peak, the abundances of CS 31082-001 in the region $38 \leq Z \leq 48$ are not all compatible with the Solar System r-process pattern. This effect is best seen in the middle and lower panels of Fig. 11, where the abundance difference $\log \epsilon_* - \log \epsilon_{r\mathrm{SS}}$ between CS 31082-001 and the Solar System (SS) r-process are

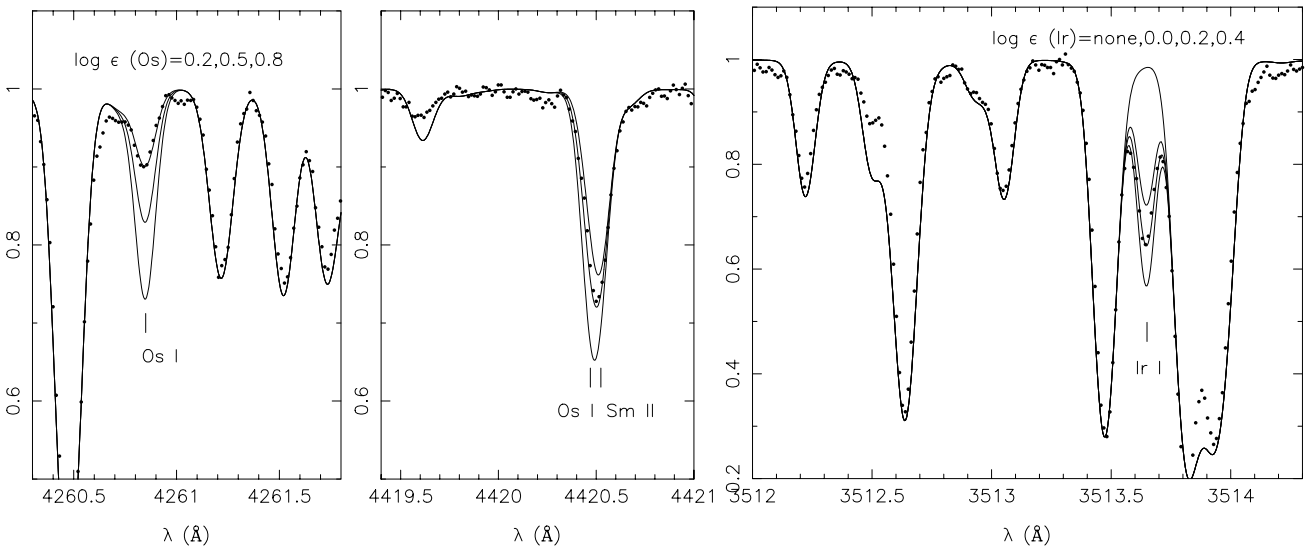

Fig. 7. The observed Os I 4261 Å, 4420 Å, and Ir I 3513 Å lines in CS 31082-001. Symbols as in Fig. 2.

displayed. When the Burris el al. (2000) de-composition is used, the difference appears as a stronger odd-even effect in CS 31082-001, in addition to a lower mean abundance: $< \log\epsilon_* - \log\epsilon_{r\rm SS} >_{38\le Z\le 48} = -1.47$ (rms 0.33) for the lighter elements vs. $< \log\epsilon_* - \log\epsilon_{r\rm SS} >_{56\le Z\le 69} = -1.25$ (rms 0.10) for the heavier group. If the Arlandini et al. (1999) de-composition is used, the result is very similar for Ru, Rh, and Ag. Note that in this case, the Y abundance is no longer discrepant, while Nb is significantly more abundant than the Solar r-value. As a result, the mean offsets between the lighter and second-peak elements over large intervals in atomic number are in fact quite similar, $<\log\epsilon_* - \log\epsilon_{r\rm SS}>_{38\le Z\le 48} = -1.38$ (rms 0.33) compared to $< \log\epsilon_* - \log\epsilon_{r\rm SS} >_{56\le Z\le 69} = -1.28$ (rms 0.08).

Independently of the decomposition used, the most discrepant element is silver, for which the solar system r-process scaled abundance exceeds the CS 31082-001 observed value by 0.8 dex! This low abundance of Ag was also observed in CS 22892-052 by Sneden et al. (2000a), and the good agreement between the CS 31082-001 and CS 22892-052 silver abundances can be seen in Fig. 12). In contrast, the only other metal-poor stars (4 halo stars with $-2.15 \le$ [Fe/H] ≤ -1.3 dex) in which it was observed so far (Crawford et al. 1998) demonstrated a mild [Ag/Fe] enhancement, in agreement with the mild enhancement of the second r-process peak elements in these stars. This illustrates that not everything is understood in the way the r-process builds up elements in the wide atomic mass-range in which it is at work.

4.4. The second-peak elements, 56 ≤ Z ≤ 72

The group of elements between barium and hafnium is the best studied mass-range of the neutron-capture elements, thanks to the relatively strong lines in the visible region of elements such as Ba, Eu, and La. In CS 31082-001 we were able to detect lines from *all* stable elements between $Z = 56$ and $Z = 72$. However, three of them cannot be used for abundance determinations because of poorly known atomic physics – Ho and Lu have very strong hyperfine structure which is not well quantified; and while three lines of Yb were detected, two are severely blended (3289 Å and 3476 Å), and the strongest one (3694 Å) yields a very large abundance ($\log\epsilon$(Yb) = 0.18), which we believe is due to the unaccounted hyperfine structure, which acts to de-saturate this strong line (123 mÅ). We are thus left with accurate abundance determinations for 13 elements in the second peak of the r-process. Figure 6 are example of the fit respectively of a Hf and a Eu line. Not that the europium hyperfine structure used here is from Kurucz (Kurucz 1993), although the oscillator strength was taken from the more recent work of Lawler et al. (2001b). The Eu isotope composition adopted was 47.8% of ^{151}Eu and 52.2% of ^{151}Eu, as in the solar system, and in accordance to the new measurement of Sneden et al. (2002) who measured this isotopic ratio to be solar in the two metal-poor r-process rich stars BD +17 3248, HD 115444 and CS 22892-052. The europium isotopic composition of CS 31082-001 will be investigated in a forthcoming paper, together with the rest of our sample of extremely metal poor stars.

The abundances of the second peak elements are displayed in Fig. 11, and compared to the Solar System r-process, scaled by the mean abundance difference with CS 31082-001: $< \log\epsilon_* - \log\epsilon_{r\rm SS} >_{56\le Z\le 69}$. Both the Burris et al. (2000) and the Arlandini et al. (1999) de-compositions are very similar in this mass range, and the mean underabundances computed for CS 31082-001 are $< \log\epsilon_* - \log\epsilon_{r\rm SS} >_{56\le Z\le 69} = -1.25$ (rms 0.10) and -1.28 (rms 0.08), respectively. The remarkable agreement of the abundance ratios in halo stars with the Solar r-process pattern in this atomic mass-range has been noted already in several papers (Sneden et al. 1996, 2000a; Westin et al. 2000; Johnson & Bolte 2001), and is also seen in giants of the globular cluster M15 (Sneden et al. 2000b). In this respect CS 31082-001 resembles

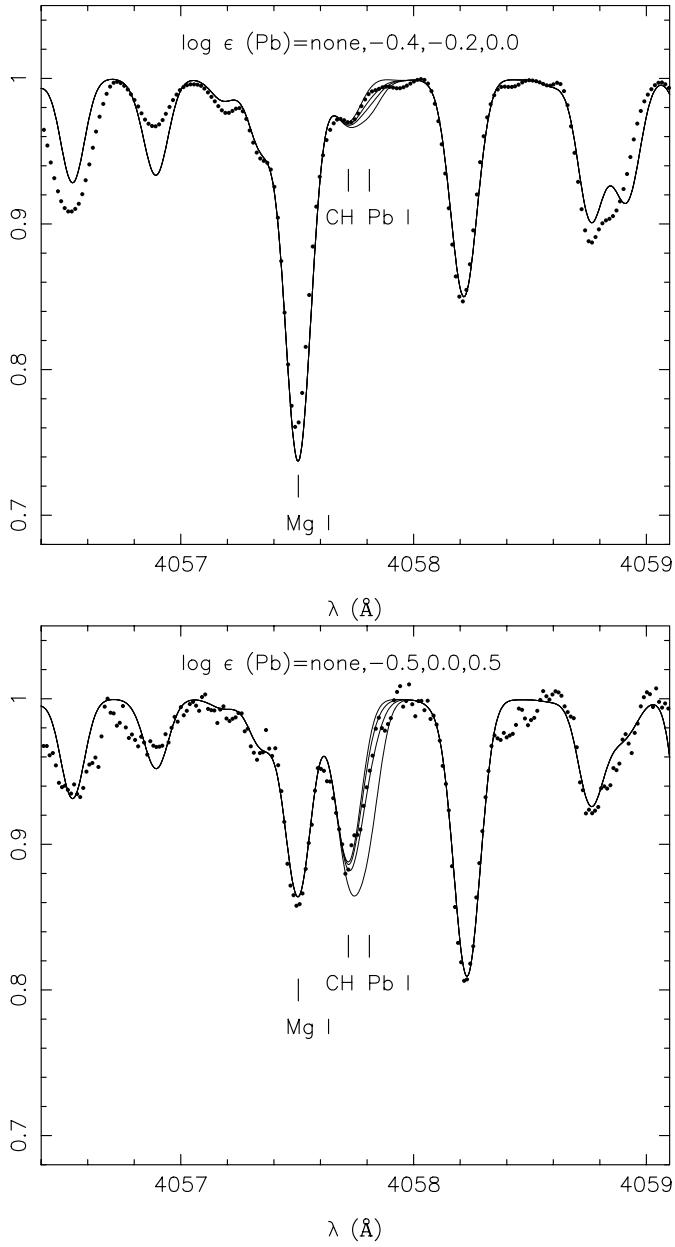

Fig. 8. The observed Pb I 4057 Å lines in CS 31082-001 (upper panel) and CS 22892-052 (lower panel). Symbols as in Fig. 2.

other metal-poor stars, both mildly r-process-enhanced (HD 115444 and others, see Johnson & Bolte 2001), and the extreme r-process-enriched star CS 22892-052. In fact, Fig. 12 shows that the neutron-capture-element pattern in CS 31082-001 (this paper) and CS 22892-052 (Sneden et al. 2000a) are virtually indistinguishable (CS 22892-052, abundances have been scaled by the mean difference between the two stars $< \log \epsilon_{\rm CS\,31082-001} - \log \epsilon_{\rm CS\,22892-052} >_{56\le Z\le 69} = +0.17$ (rms 0.10)). Note that while the absolute r-process abundances are larger in CS 31082-001, given the metallicity difference between the two stars ($[{\rm Fe/H}]_{\rm CS\,31082-001} = -2.9$ and $[{\rm Fe/H}]_{\rm CS\,22892-052} = -3.2$), the total $[r/{\rm Fe}]$ ratio in CS 31082-001 in the mass range $56 \le Z \le 69$ is 0.13 dex lower than in CS 22892-052.

4.5. The third-peak elements and the actinides, $76 \le Z \le 92$

The third r-process peak (near the magic number $N = 126$) is sampled in CS 31082-001 by Os and Ir. The two heaviest species detected are the radioactive actinides Th and U, the use of which as chronometers we discuss in Sect. 6.

Osmium and iridium

Figure 7 shows two of the three osmium detections, and one of the two iridium detections. It was suggested in our preliminary results (Hill et al. 2001) that these two elements were overabundant with respect to the Solar r-process by around +0.3 dex. We now revise this statement slightly. In particular, Ir falls back to the same abundance scale as the $56 \le Z \le 69$ elements. The reason for this revision is connected with the code used to derive abundances. In our preliminary analysis (Hill et al. 2001) we were using the code of Spite (1967), while in the present analysis we have switched to a more self-consistent approach, the synthesis code by Plez et al. (1993), which employs the same algorithms to compute the model atmosphere and the synthetic spectrum. The main difference between the two codes lies in the continuous opacity computations and the source function assumptions (a diffusive term is added in the latter). These codes provide identical results above 4000 Å (less than 0.02 dex difference), but the present, presumably more reliable approach, yields systematically lower abundances in the bluest part of the spectrum (with a maximum effect of ∼0.2 dex). In the case of Ir, the two lines at 3512 Å and 3800 Å gave discrepant results in our preliminary analysis, but now agree, with $\log \epsilon({\rm Ir}) = 0.2$ dex (instead of the earlier 0.37 dex which came from the 3512 Å line alone).

Osmium, on the other hand, still seems to be overabundant with respect to both the scaled Solar r-process fraction and to CS 22892-052. If Os in CS 31082-001 was enhanced to the same level as the second r-process peak elements, we would expect $\log \epsilon({\rm Os}) = 0.15$ dex, and $\log \epsilon({\rm Os}) = 0.12$ dex if it was enhanced similarly to CS 22892-052, whereas we observe $\log \epsilon({\rm Os}) = 0.43$ dex (rms 0.17, from 3 lines). We investigated the possible source of differences between our analysis and that of Sneden et al. (1996, 2000a), which could explain this difference: (i) The three lines used here are the same as those used by Sneden et al. (same wavelengths, same excitation potential and same oscillator strengths), (ii) the ionisation potential of Os I adopted here is from a measurement by Colarusso et al. (1997) of 8.44eV, compared to 8.35eV adopted by Sneden et al. (1996), which could account for at most ∼0.1 dex difference in the final abundance but in the wrong direction, (iii) the difference in the codes used for the abundance determination cannot play a role *only for osmium*, leaving all the other abundance determinations unaffected. Hence, at this point, we cannot account for the abundance discrepancy by any obvious differences in the analysis.

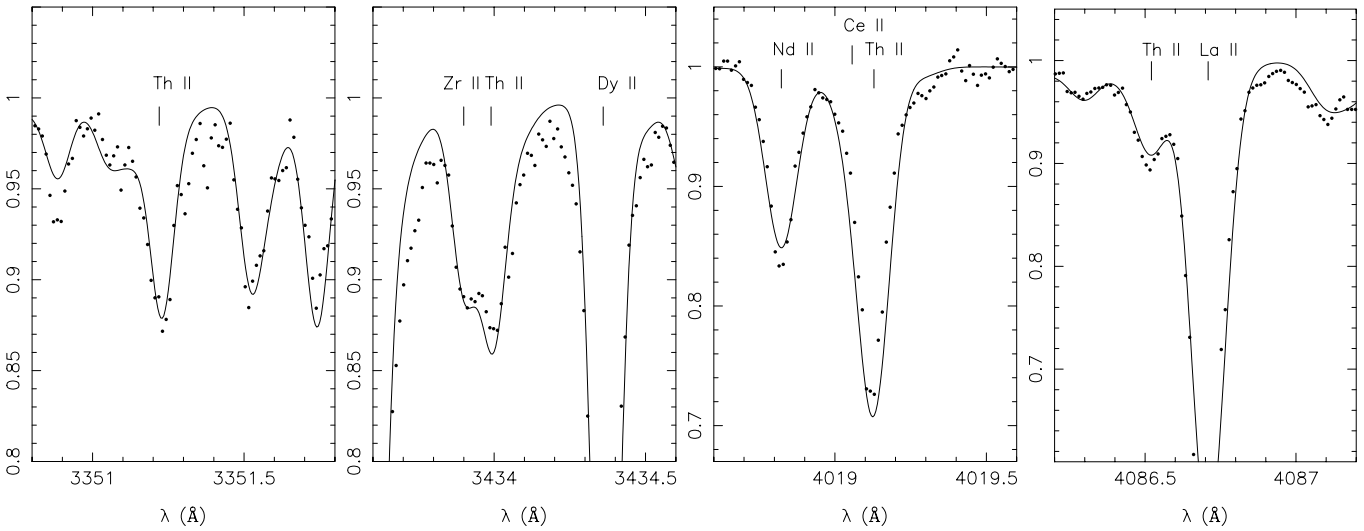

Fig. 9. The observed Th II 3351 Å, 3434 Å, 4019 Å and 4086 Å lines in CS 31082-001. *Dots*: observations; *line*: synthetic spectrum computed for the mean Th abundance, $\log\epsilon(\mathrm{Th}) = -0.98$.

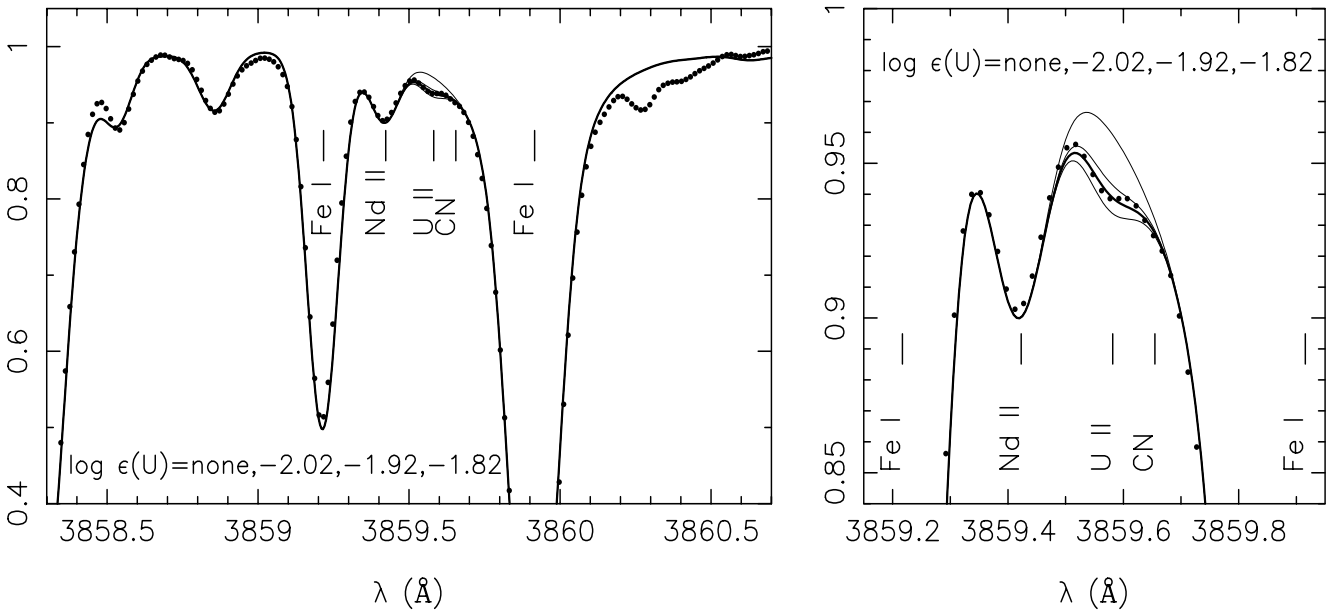

Fig. 10. The observed U II 3859 Å line in CS 31082-001. Symbols as in Fig. 2. The best fit is found for $\log\epsilon(\mathrm{U}) = -1.92$ (thick line).

We are therefore left with the possibility that the Os content of CS 31082-001 is indeed larger than predicted by a scaled Solar r-process. On the other hand, the large abundance dispersion observed from the three lines (rms 0.17) is a hint that there may be hidden problems in the determination of Os abundance from these lines, so that any strong conclusion would be premature at this stage.

Lead

Recently, accurate abundances of lead in metal-poor CH stars (the Pb having likely been transferred from a now-extinct AGB companion) were reported by Aoki et al. (2000) and Van Eck et al. (2001), using the 4057.8 Å line. In CS 31082-001, this line is not visible. Hence, we can only assign an upper limit of $\log\epsilon(\mathrm{Pb}) < -0.2$ dex ($\log\epsilon(\mathrm{Pb}) = -0.4^{+0.2}_{-\infty}$), as shown in Fig. 8. However, even this upper limit is of great interest, since it is already *below* the expected abundance of the scaled Solar System r-process fraction (Fig. 11).

Noting from Fig. 12 that our derived abundance of Pb is drastically lower than the detection reported by Sneden et al. (2000a) for CS 22892-052, we re-assessed also the abundance of Pb in CS 22892-052 from spectra taken with VLT+UVES during the commissioning of the instrument (`http://www.eso.org/science/uves_comm/`). The spectrum was acquired with a resolution of $R = 55\,000$; the S/N of the co-added spectrum (total exposure time of 4.5 h) is ∼140 per (0.013 Å) pixel at 4100 Å (i.e., $S/N \sim 330$ per resolution element). The model for CS 22892-052 is an OSMARCS model with

$T_{\rm eff}$ = 4700 K, $\log g$ = 1.5, [Fe/H] = −3.0 and [α/Fe] = +0.40 (following Sneden et al. 2000a). The syntheses were generated with ξ = 2.1 km s^{-1}, [Fe/H] = −3.2, and individual abundances from Sneden et al. (1996). C and N abundances were determined, through a fit of the 3850–3900 Å region (CH and CN bandheads), to be $\log\epsilon$(C) = 6.07 ([C/Fe] = +0.75) and $\log\epsilon$(N) = 5.42 ([N/Fe] = +0.70). Then the Pb region was synthesized (some *gf* values of nearby atomic lines were adjusted to fit the observed spectrum). The Pb line lies in the red wing of a CH line, which is nicely fitted with the abundances derived from the 3850–3900 Å region. Spectra were computed for $\log\epsilon$(Pb) = −0.5, 0.0, 0.5, and no Pb. From inspection of Fig. 8 we derive an upper limit for the Pb abundance of $\log\epsilon$(Pb)< 0.0 ($\log\epsilon$(Pb) = $-0.25^{+0.25}_{-\infty}$). The Pb contents of CS 22892-052 and CS 31082-001, therefore, do not seem to be very different, and the reality of the measurement by Sneden et al. (2000a) appears open to question.

Thorium and uranium

The oscillator strengths of the single U II line and eight of the Th II lines that we have measured in CS 31082-001 (Table 4), as well as many others, have been re-determined with superior accuracy by Nilsson et al. (2001a, 2001b). The associated change in the U/Th abundance ratio is quite significant, as the oscillator strengths of the Th II lines decrease by 0.07 dex, on average, whereas the $\log gf$ of the U II line increases from −0.20 to −0.067, i.e., by 0.13 dex. Moreover, the uncertainties associated with the oscillator strengths have been reduced drastically (to better than 0.08 dex for the individual Th lines, and to only 0.06 dex for the U II line), thus they are a negligible source of error compared to the uncertainties in the actual fit of the data. Figure 9 displays the synthesis of a selection of the observed thorium lines, all plotted with a thorium abundance equal to the mean of the eight lines ($\log\epsilon$(Th) = −0.98). The observed uncertainty in this case was estimated as $\sigma/\sqrt{N-1}$, where σ is the dispersion around the mean and N, the number of lines, hence leading to a $\log\epsilon$(Th) = -0.98 ± 0.02.

Figure 10 shows the region of the U II 3859 Å line and an enlargement of the uranium line itself, together with synthetic spectra for four different uranium abundances. The accuracy of the fit is estimated to be around 0.1 dex, obtained by testing the influence of several potential sources of error on the fitting procedure, including placement of the continuum and blending by neighboring lines (mainly Fe I 3859.9 Å). The uncertainty arising from the blending of the Fe I line is linked to uncertainties on the oscillator strength, but also the broadening factor of the line. The Van der waals broadening factor was taken from Barklem et al. (1998), and the oscillator strength was increased by 0.1 dex with respect to the VALD2 recommended value to give a best fit to the observed line Fe I 3859.9 Å. Attempts to vary the Barkelem damping constant by 5% or more induced changes in the U abundance of less than 10%. The unidentified features on the red side of the line (at 3860.77 and 3860.9 Å respectively) hamper the cosmetics of the fit but have no influence on the uranium line region. We would like to point out that the 3860.77 Å unidentified line also appears in the spectrum of CS 22892-052, whereas it does not in other giants of similar metallicity and temperature which have no excess of neutron-capture elements. We therefore tentatively attribute this absorption feature to an neutron-capture element, and encourage atomic physicists to work on the identification of this feature. We also note here that there are numerous features in the whole UV part of the spectrum of neutron-capture enriched giants, that are still in need of identification. A more detailed analysis of the 5-line feature (Fe I 3859.21, Nd II 3859.4, U II 3859.57, CN 3859.67 and Fe I 3859.9 Å) is forseen is a near future, involving 3D hydrodynamical models. Adding the 0.06 dex uncertainty associated with the $\log gf$ of the line results in $\log\epsilon(U) = -1.92 \pm 0.11$. As seen from Table 6, the overall uncertainty of the U/Th ratio is totally dominated by that of the U line fitting procedure, while errors in the stellar parameters cancel out completely.

Finally, we note that, using the newly determined oscillator strength value for the uranium line, the upper limit deduced by Gustafsson & Mitzuno-Wiedner (2001) for CS 22892-052 becomes $\log\epsilon$(U) ≤ −2.54.

5. Is the r-process universal?

From the discussion in the previous section, and from Figs. 11 and 12, it is clear that the neutron-capture elements in CS 31082-001 follow a standard pattern (i.e., they are indistinguishable from both the scaled Solar r-process pattern and the patterns observed in other metal-poor halo stars such as CS 22892-052) for elements $56 \leq Z \leq 72$. The small dispersion around the mean of the quantities ($\log\epsilon_{\rm CS\,31082-001} - \log\epsilon_{\rm CS\,22892-052}$) and ($\log\epsilon_{\rm CS\,31082-001} - \log\epsilon_{r_{\rm SS}}$) in the range $56 \leq Z \leq 69$ (respectively 0.10 and 0.08 dex) reflect this level of agreement.

In CS 31082-001, the third neutron-capture peak is so far only sampled by abundance measurements of two elements (Os and Ir), and one upper limit (Pb). There may be marginal evidence for departure from the Solar r-process (Os seems overabundant), but it is premature to conclude firmly on this point (see Sect. 4.5). The third-peak abundance determinations clearly demand confirmation from better measurements and laboratory data (Os), and from new detections (Pt, Pb, Bi), which can only be done from space, as the strongest lines of these elements are too far in the UV region to be reached from the ground.

On the other hand, the actinides, although only probed by the two radioactive nuclides Th and U, do appear to be enhanced in CS 31082-001 to a higher level than observed for elements of the second r-process peak. Given the very high ratios of log(Th/Eu) = −0.22 dex (where Eu is taken as a typical example of the elements $56 \leq Z \leq 69$) compared to other halo stars (for example, CS 22892-052 with log(Th/Eu) = −0.66, and HD 115444 with

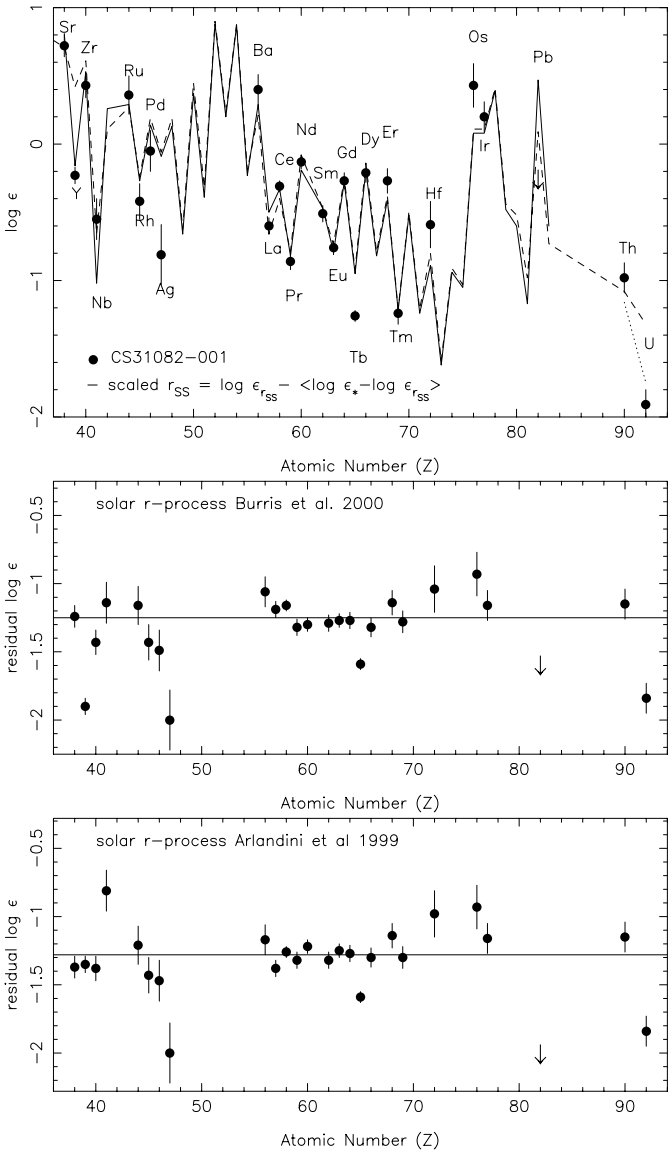

Fig. 11. *Top*: neutron-capture-element abundances of CS 31082-001 compared to the Solar System r-process scaled to match the $56 \leq Z \leq 69$ elemental abundances of CS 31082-001. Two sources are plotted for the Solar r-process: Burris et al. 2000 (dashed line) and Arlandini 1999 (full line). Note that the radioactive species (Th and U) Solar System abundances are corrected for radioactive decay since the formation of the Solar System. The dotted line show the abundances observed *today* for these two species (scaled in the same manner). *Middle*: residual abundance of CS 31082-001 after the Solar System r-process (Burris et al. 2000) has been subtracted. *Bottom*: residual abundance of CS 31082-001 after the Solar System r-process (Arlandini et al. 1999) has been subtracted.

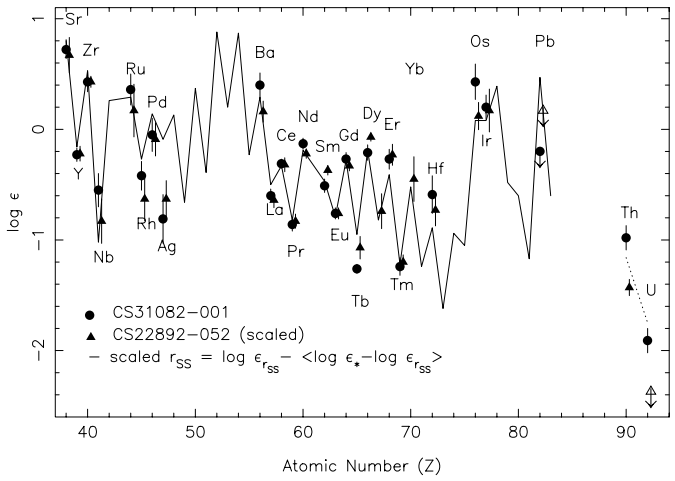

Fig. 12. Neutron-capture-element abundances of CS 31082-001 compared to CS 22892-052 (Sneden et al. 2000a). The abscissa for CS 22892-052 has been artificially shifted by +0.3 for readability, and the abundances were scaled up by $< \log \epsilon_{\rm CS\,31082-001} - \log \epsilon_{\rm CS\,22892-052} >_{56 \leq Z \leq 69} = +0.17$dex. The two open symbols are our own estimates for the Pb and U content of CS 22892-052 (see Sect. 4.5). The full line is the Solar r-process fraction from Arlandini et al. (1999).

$\log(\mathrm{Th/Eu}) = -0.60$) it is difficult to conceive any reasonable scenario that would account for this by an age difference: CS 22892-052 and HD 115444 would then be 20 and 18 Gyrs older than CS 31082-001, respectively (regardless of the adopted production ratio for Th/Eu), which seems unrealistic.

We are thus left with the possibility that the actinides were enhanced ab initio by a larger factor than the elements of the second r-process peak in the matter that gave birth to CS 31082-001. This is the first time that such a large departure (∼0.4 dex) from the otherwise standard Solar r-process pattern has been observed in a halo star, and the implications are important. *If the actinides are not necessarily produced together with the lighter neutron-capture elements (*$56 \leq Z \leq 72$*), and their initial proportions are therefore not fixed, but instead vary from star to star, then any chronometer based on ratios of an actinide to any stable element from the second r-process peak is doomed to failure.* The Th/Eu ratio in CS 31082-001 is an extreme example of such a failure (see Sect. 6).

From the r-process modeling point of view, the de-coupling of the production of actinides from the production of lighter r-process elements is in fact not unexpected. Goriely & Arnould (2001) find in their superposition of CEVs (Canonical EVents) that reproduce the Solar r-process pattern, that *the CEVs that are responsible for the synthesis of the actinides do not contribute to the synthesis of nuclides lighter than Pb.* This point is considered in more detail by Schatz et al. (2002).

As a final remark, we compared abundances of all elements from Na to U, to the predictions of the Qian & Wasserburg (2001b, 2002) phenomenological model which describes the chemical enrichment in the early galaxy in terms of three components: the prompt enrichment (P) is the contribution from extremely massive stars and acts on an instantaneous timescale, and SN II are divided in two classes, the high-frequeny SN II (H) and low-frequency SN II (L) are responsible respectively for the second and third r-process peak elements, and for some iron and light

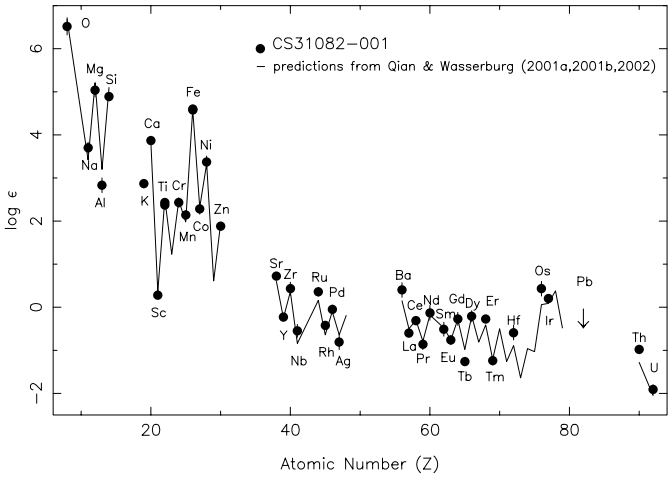

Fig. 13. Abundances of CS 31082-001 compared to the predictions of Qian & Wasserburg (2001b, 2002) three component phenomenological model.

r-process elements. As in Qian & Wasserburg (2001a), the total number of H events that contributed to the abundances of CS 31082-001 can be computed as $n_{\rm H} \simeq 52$ from the observed Eu abundance in this star (predictions for the other r-process elements are made according to empirical yields determined from the observed neutron-capture elements abundances in CS 22892-052 and HD 115444), while the P component is responsible for all elements Na-Zn (where the yields are computed in Qian & Wasserburg (2002) directly from the observed abundances of extremely metal poor stars, HD 115444 in this case). The overall excellent agreement between the observed abundances in CS 31082-001 and the predictions of Qian & Wasserburg seen in Fig. 13 is therefore showing primarily, (i) that the abundances Na-Zn of CS 31082-001 are in very good agreement with *normal* extremely metal poor stars; (ii) that the neutron-capture pattern up to $Z = 70$ is also in very good agreement with their H yields (i.e. very close to the abundances of CS 22892-052) and (iii) that the Os, Th and U abundances are above the predictions, as previously discussed in this section.

6. The age of CS 31082-001

The very low metallicity of CS 31082-001, well below that of the most metal-poor globular clusters, shows that it was formed in the earliest star formation episodes, either in the Galaxy or in a substructure which later merged with the Galaxy. Comparison with the metallicity of damped Ly-α systems at high redshift (Lu et al. 1996; Vladilo et al. 2000) shows that the matter in CS 31082-001 probably originated at an epoch earlier than $z = 5$. Assuming $\Omega_0 = 0.3$, H_0 in the plausible range 65–75 km s^{-1}/Mpc, and a flat geometry (de Bernardis et al. 2000), the Big Bang occurred about 0.5 Gyr before the epoch $z = 10$, and 1 Gyr before $z = 5$. Accordingly, the age of the progenitor of CS 31082-001, as determined from the U/Th clock, provides a lower limit to the age of the Universe which is *very* close to that age itself.

Dating matter from the decay of a radioactive isotope is simple in principle, provided that the ratio of the radioactive nuclide to a stable reference element produced at the same time can be inferred. Let $(R/S)_0$ be the initial production ratio of a radioactive nuclide, R, to a stable one, S, and $(R/S)_{\rm now}$ be the value of that ratio observed today. The time for R/S to decay by a factor of 10 is then $\tau_{10} = \tau/\log(2)$, where τ is the half-life of R. For ^{232}Th and ^{238}U (τ = 14.05 and 4.47 Gyr, respectively), this yields the following expressions for the time Δt (in Gyrs) elapsed since the production of these elements:

$$\Delta t = 46.67[\log({\rm Th/S}_0) - \log({\rm Th/S}_{\rm now})] \quad (1)$$

$$\Delta t = 14.84[\log({\rm U/S}_0) - \log({\rm U/S}_{\rm now})]. \quad (2)$$

These relations show that, if the right-hand sides can be evaluated to a realistic accuracy of 0.1 dex, the corresponding error on Δt becomes 4.7 Gyr for Th and 1.5 Gyr for U, demonstrating immediately the huge advantage of U over the previously used Th in cosmochronometry. However, finding a stable r-process element that permits a spectroscopic determination of $(R/S)_{\rm now}$ and a theoretical prediction of $(R/S)_0$, with a *combined overall* error of 0.1 dex is a significant, unsolved problem.

Hence, we look to an obvious alternative. Substituting Th for the stable element S in Eq. (2) above, we obtain:

$$\Delta t = 21.76[\log({\rm U/Th}_0) - \log({\rm U/Th}_{\rm now})]. \quad (3)$$

Thus, for a given uncertainty in the decay of the U/Th ratio, the error in Δt is 50% larger than for U alone, but still a factor of two better than for Th alone. Adopting the slightly radioactive, but structurally very similar Th, as the reference element for U leads to great gains in accuracy of both terms on the right-hand side of Eq. (3). First, the ionization and excitation potentials of the atomic levels giving rise to the observed spectral lines are similar, so that errors in the model atmospheres and assumed parameters largely cancel in the ratio U/Th (see Table 6). Second, the initial production ratio of the neighboring nuclides ^{238}U and ^{232}Th should be far less sensitive to variations in the poorly-known characteristics of the neutron exposure(s) occurring in the explosion of progenitor than the ratios of nuclides more widely separated in mass, such as ^{232}Th and $^{151-153}$Eu (Goriely & Clerbaux 1999).

Much progress has already been made on both fronts since the publication of our discovery paper (Cayrel et al. 2001). First, the oscillator strengths of the single U II line and eight of the Th II lines that we have measured in CS 31082-001 have been re-determined (Sect. 4.5). The change in the U/Th abundance ratio is quite significant, revising the log(U/Th) from the previous value of -0.74 ± 0.15 to -0.94 ± 0.11. Using the same initial production ratio as in Cayrel et al. (2001), this leads to an age of almost 17 Gyr, 4.3 Gyr greater than that originally published. By contrast, use of the conventional Th/Eu chronometer

(Cowan et al. 1999) leads instead to a slightly negative (!), or at most a T-Tauri like age for CS 31082-001.

Fortunately, there has also been progress regarding predictions of the initial production ratio for these elements. In a recent paper, Goriely & Arnould (2001) review in great detail the production of the actinides in the light of the Solar System data. Although they conclude that no current solution explains the Solar System data exactly, stretching the lower and upper limits of the production ranges by just 0.1 dex makes 10 of the 32 cases they consider acceptable. The corresponding production ratios range from 0.48 to 0.54, with a mean of 0.50 ± 0.02, close to the value of 0.556 (from Cowan et al. 1999) cited by Cayrel et al. (2001). Combined with our newly measured U/Th ratio, this leads to an age of 14.0 ± 2.4 Gyr for the Th and U in CS 31082-001 (where the error refers only to the uncertainty on the observed U/Th ratio). This is a quite reasonable value, inspiring some hope that the predicted production ratio of U/Th is fairly robust.

At this point, it is impossible to assign a reliable error estimate to this age, given the lack of observational constraints on the production ratio of U/Th from other species that might have experienced the same neutron exposure. Verification of the predicted abundances of the decay products Pb and Bi, the direct descendants of U and Th, is therefore of particular importance. No useful lines of these elements are measurable, even in our high-quality VLT/UVES spectra of CS 31082-001, and we suspect that they may remain unmeasurable, regardless of improvements in future ground-based facilities. Fortunately, time on the Hubble Space Telescope has been assigned to obtain a high-resolution UV spectrum of CS 31082-001, where the strong resonance lines of these species might indeed be detected.

Let us note also that using the upper limit $\log \epsilon(\mathrm{U}) \leq -2.54$ of Gustafsson & Mitzuno-Wiedner (2001, modified to account for the new gf of the U line) for uranium in CS 22892-052, and the thorium abundance $\log \epsilon(\mathrm{Th}) = -1.60$ of Sneden et al. (2000a), the ratio $\mathrm{U/Th} \leq -0.94$ in CS 22892-052 is fully compatible with the one of CS 31082-001. Hence, despite a difference in the overall thorium content of the two stars, their ages derived from the U/Th ratio is fully consistent.

7. Conclusions and future work

The apparent brightness, very low [Fe/H], and enormous r-process enhancement, in combination with the lack of molecular blanketing, makes CS 31082-001 a uniquely favorable object for study of the r-process nucleosynthesis history in the early Galaxy. The most conspicuous result of these characteristics is the breakthrough in the measurement of the abundance of uranium in this very old star, facilitated by our excellent VLT/UVES spectra, which enable the determination of accurate abundances for 41 (plus 2 upper limits – N and Pb – and 3 detections which could not be translated into accurate determinations – Ho, Lu and Yb – due to a lack of input atomic physics) other elements as well. But the importance of CS 31082-001 extends further, as it has provided the first solid evidence that variations in progenitor mass, explosion energy, distance to dense interstellar clouds, and/or other intrinsic and environmental factors preceding the formation of the extreme halo stars, may produce significantly different r-process abundance patterns from star to star in the actinide region ($Z \geq 90$).

A striking consequence of these variations is the *complete failure of the conventional Th/Eu chronometer* in CS 31082-001, assuming an initial production ratio for the pair as in CS 22892-052, or as in the r-process elements of the Solar System. No such problem is seen for the pair U/Th, which leads to an age of 14.0 ± 2.4 Gyr (not including systematic errors in the initial production ratio). This suggests that the closely similar masses and nuclear structures of ^{238}U and ^{232}Th lead to a more stable production ratio between these two nuclides than, e.g., that of ^{232}Th and $^{151-153}$Eu. However, further studies are needed of the robustness of the U/Th ratio produced by exposing iron nuclei to neutron exposures of various strengths, as well as of the abundances of the daughter elements of their decay, Pb and Bi.

Observations in CS 31082-001 itself of the Pb and Bi created in the same neutron exposure event as U and Th, and by their subsequent decay, will be particularly crucial as constraints on the predicted production ratios of all r-process elements. Of equal importance is the continuation of searches for new r-process-enhanced metal-poor stars, so that better measures of the star-to-star variation in the observed patterns of the r-process elements, in particular those of the third-peak and the actinides, may be obtained.

Acknowledgements. This research has made use of the Simbad database, operated at CDS, Strasbourg, France. We are grateful to Pr. Johansson and his group for their timely response to our request for accurate lifetime measurements of uranium and thorium electronic levels. BN and JA thank the Carlsberg Foundation and the Swedish and Danish Natural Science Research Councils for financial support for this work. T.C.B acknowledges partial support from grants AST 00-98549 and AST 00-98508 from the U.S. National Science Foundation.

Appendix A: Line list and atomic data

We list in this table all the lines of neutron-capture elements that were used to derive abundances. The wavelengths, excitation potentials, and oscillator strengths are listed, together with references for the oscillator strengths. Also listed are the equivalent widths of the lines in CS 31082-001, and the derived abundances. The word "syn" in Col. 5 denotes that spectral synthesis techniques were used rather than the equivalent width to derive the abundance.

Table A.1. Linelist, equivalent width and abundances for the neutron-capture elements in CS 31082-001.

λ (Å)	Exc. Pot. (eV)	$\log gf$	Ref.	W (mÅ)	$\log\epsilon$
Sr II					
4077.709	0.00	0.170	1	syn	0.70
4161.792	2.94	−0.600	1	syn	0.75
4215.519	0.00	−0.170	1	syn	0.70
Y II					
3774.331	0.13	0.210	2	86.0	−0.29
3788.694	0.10	−0.070	2	83.0	−0.14
3818.341	0.13	−0.980	2	45.0	−0.15
3950.352	0.10	−0.490	2	69.4	−0.16
4398.013	0.13	−1.000	2	45.0	−0.23
4883.684	1.08	0.070	2	42.4	−0.27
5087.416	1.08	−0.170	2	28.6	−0.32
5123.211	0.99	−0.830	2	10.6	−0.30
5200.406	0.99	−0.570	2	19.8	−0.25
5205.724	1.03	−0.340	2	26.0	−0.28
Zr II					
3836.762	0.56	−0.060	3	61.0	0.24
4161.213	0.71	−0.720	3	40.0	0.57
4208.977	0.71	−0.460	3	45.0	0.40
4317.299	0.71	−1.380	3	13.0	0.54
4496.980	0.71	−0.590	3	35.0	0.30
Nb II					
3215.591	0.44	−0.190	4[a]	syn	−0.55
Ru I					
3436.736	0.15	0.015	5[a]	syn	0.40
3498.942	0.00	0.310	5[a]	syn	0.28
3728.025	0.00	0.270	5[a]	syn	0.20
3798.898	0.15	−0.040	5[a]	syn	0.40
3799.349	0.00	0.020	5[a]	syn	0.45
Rh I					
3396.819	0.00	0.050	4[a]	syn	−0.40
3434.885	0.00	0.450	4[a]	syn	−0.45
3692.358	0.00	0.174	4[a]	syn	−0.40
Pd I					
3242.700	0.81	−0.070	4[a]	syn	0.00
3404.579	0.81	0.320	4[a]	syn	−0.18
3634.690	0.81	0.090	4[a]	syn	0.00
Ag I					
3280.679	0.00	−0.050	4[a]	syn	−0.95
3382.889	0.00	−0.377	4[a]	syn	−0.70
Ba II					
3891.776	2.51	0.280	6	syn	0.15
4130.645	2.72	0.560	6	syn	0.20
4554.029	0.00	0.170	6	syn	0.40
4934.076	0.00	−0.150	6	syn	0.60
5853.668	0.60	−1.010	6	syn	0.50
6141.713	0.70	−0.070	6	syn	0.40
La II					
3849.006	0.00	−0.450	7[a]	syn	−0.60
4086.709	0.00	−0.070	7[b]	syn	−0.55
4123.218	0.32	0.130	7[b]	syn	−0.65
5122.988	0.32	−0.850	7[b]	syn	−0.58
6320.376	0.17	−1.520	7[b]	7.0	−0.61
Ce II					
4073.474	0.48	0.320	8	26.3	−0.45
4083.222	0.70	0.240	8	21.0	−0.24
4120.827	0.32	−0.240	8	16.0	−0.37
4127.364	0.68	0.240	8	21.0	−0.27
4222.597	0.12	−0.180	1	33.0	−0.25
4418.780	0.86	0.310	8	14.0	−0.38
4486.909	0.30	−0.360	1	22.0	−0.14
4562.359	0.48	0.330	1	31.0	−0.41
4628.161	0.52	0.260	1	26.6	−0.40
Pr II					
3964.262	0.22	−0.400	8	syn	−0.80
3964.812	0.05	0.090	9	28.0	−0.99
3965.253	0.20	−0.130	9	18.0	−0.84
4062.805	0.42	0.330	10	37.0	−0.70
5220.108	0.80	0.170	9	7.3	−1.01
5259.728	0.63	−0.070	9	8.1	−0.93
Nd II					
3973.260	0.63	0.430	11	syn	−0.17
4018.823	0.06	−0.880	12	19.0	−0.20
4021.327	0.32	−0.170	13	35.0	−0.22
4061.080	0.47	0.300	11	62.0	0.07
4069.265	0.06	−0.400	13	34.4	−0.32
4109.448	0.32	0.180	11	syn	0.15
4232.374	0.06	−0.350	13	34.5	−0.39
4446.384	0.20	−0.630	12	35.0	0.04
4462.979	0.56	−0.070	11	38.0	−0.03
5130.586	1.30	0.100	11	13.3	−0.00
5212.361	0.20	−0.700	13	14.6	−0.48
5234.194	0.55	−0.460	12	16.0	−0.25
5249.576	0.98	0.080	14	20.0	−0.16
5293.163	0.82	−0.200	14	21.3	−0.04
5311.453	0.99	−0.560	14	5.4	−0.16
5319.815	0.55	−0.350	14	27.7	−0.06
5361.467	0.68	−0.400	13	12.6	−0.29
5442.264	0.68	−0.900	13	4.2	−0.31
Sm II					
3793.978	0.10	−0.500	15	19.0	−0.71
3896.972	0.04	−0.580	15	21.0	−0.66
4023.222	0.04	−0.830	15	16.0	−0.57
4068.324	0.43	−0.710	15	7.0	−0.65
4318.927	0.28	−0.270	15	33.0	−0.45
4499.475	0.25	−1.010	15	13.0	−0.30
4519.630	0.54	−0.430	15	18.0	−0.37
4537.941	0.48	−0.230	15	16.0	−0.71
4577.688	0.25	−0.770	15	18.0	−0.38

Table A.1. continued.

λ (Å)	Exc. Pot. (eV)	$\log gf$	Ref.	W (mÅ)	$\log\epsilon$
Eu II					
3724.931	0.00	−0.090	16[b]	syn	−0.59
3930.499	0.21	0.270	16[b]	syn	−0.78
3971.972	0.21	0.270	16[b]	syn	−0.84
4129.725	0.00	0.220	16[b]	syn	−0.77
4205.042	0.00	0.210	16[b]	syn	−0.66
4435.578	0.21	−0.110	16[b]	syn	−0.76
4522.581	0.21	−0.670	16[b]	syn	−0.91
6437.640	1.32	−0.320	16[b]	syn	−0.88
6645.064	1.38	0.120	16[b]	3.0	−0.72
Gd II					
3768.396	0.08	0.250	17	61.0	−0.33
3796.384	0.03	0.030	18	63.0	−0.13
3836.915	0.49	−0.320	4[a]	19.0	−0.27
3844.578	0.14	−0.510	17	30.0	−0.22
3916.509	0.60	0.060	17	22.0	−0.45
4037.893	0.73	0.070	18	15.0	−0.53
4085.558	0.56	−0.230	18	17.0	−0.37
4130.366	0.73	0.140	18[a]	25.0	−0.32
4191.075	0.43	−0.680	17	18.0	−0.06
Tb II					
3658.886	0.13	−0.010	19[b]	12.5	−1.27
3702.853	0.13	0.440	19[b]	33.0	−1.19
3848.734	0.00	0.280	19[b]	38.0	−1.34
3874.168	0.00	0.270	19[b]	29.0	−1.19
3899.188	0.37	0.330	19[b]	17.0	−1.23
4002.566	0.64	0.100	19[b]	4.0	−1.38
4005.467	0.13	−0.020	19[b]	17.3	−1.23
Dy II					
3869.864	0.00	−0.940	20	29.3	−0.21
3996.689	0.59	−0.190	20	32.6	−0.20
4011.285	0.93	−0.630	20	5.5	−0.32
4103.306	0.10	−0.370	20	61.2	−0.01
4468.138	0.10	−1.500	20	8.5	−0.27
5169.688	0.10	−1.660	20	5.5	−0.38
Er II					
3692.649	0.05	0.138	21	syn	−0.25
3786.836	0.00	−0.640	21	46.0	−0.26
3830.482	0.00	−0.360	21	58.5	−0.26
3896.234	0.05	−0.240	22	64.0	−0.19
3938.626	0.00	−0.520	8	38.0	−0.40
Tm II					
3700.256	0.03	−0.290	8	25.0	−1.28
3761.333	0.00	−0.250	8	syn	−1.10
3795.760	0.03	−0.170	8	28.0	−1.34
3848.020	0.00	−0.520	8	syn	−1.25
Hf II					
3399.793	0.00	−0.490	23	syn	−0.50
3719.276	0.61	−0.870	8	syn	−0.70
Os I					
4135.775	0.52	−1.260	8	9.0+syn	0.52
4260.848	0.00	−1.440	8	12.0+syn	0.21
4420.468	0.00	−1.530	24	syn	0.50
Ir I					
3513.648	0.00	−1.260	4[a]	34.0+syn	0.20
3800.120	0.00	−1.450	4[a]	syn	0.20
Pb I					
4057.807	1.32	−0.170	25[a]	syn	<-0.2

Table A.1. continued.

λ (Å)	Exc. Pot. (eV)	$\log gf$	Ref.	W (mÅ)	$\log\epsilon$
Th II					
3351.229	0.19	−0.600	26[a]	7.0+syn	−0.95
3433.999	0.23	−0.537	26[a]	10.0+syn	−1.05
3435.977	0.00	−0.670	26[a]	14.0+syn	−1.05
3469.921	0.51	−0.129	26[a]	10.0+syn	−1.00
3675.567	0.19	−0.840	26[a]	5.0+syn	−0.92
4019.129	0.00	−0.228	26[a]	31.0+syn	−1.03
4086.521	0.00	−0.929	26[b]	10.0+syn	−0.95
4094.747	0.00	−0.885	26[a]	7.0+syn	−0.95
U II					
3859.571	0.036	−0.067	27[a]	syn	−1.92

[a] Not in Sneden et al. (1996).
[b] $\log gf$ different than in Sneden et al. (1996).
1: Gratton & Sneden (1994); 2: Hannaford et al. (1982); 3: Biémont et al. (1981); 4: VALD: Bell heavy; 5: Wickliffe et al. (1994); 6: Gallagher (1967); 7: Lawler et al. (2001a); 8: Sneden et al. (1996) (From Kurucz compilation); 9: Goly et al. (1991); 10: Goly et al. (1991), Lage & Whaling (1976); 11: Maier & Whaling (1977); 12: Ward et al. (1984, 1985), modified (Sneden et al. 1996); 13: Corliss & Bozman (1962), modified (Sneden et al. 1996); 14: Maier & Whaling (1977), Ward et al. (1984, 1985); 15: Biemont et al. (1989); 16: Lawler et al. (2001b); 17: Corliss & Bozman (1962); 18: Bergström et al. (1988); 18: Bergstrom et al. (1988); 19: Lawler et al. (2001c); 20: Kusz (1992), Biémont & Lowe (1993); 21: Musiol & Labuz (1993); 22: Biémont & Youssef (1984); 23: Andersen et al. (1975); 24: Kwiatkowski et al. (1984); 25: Reader & Sansonetti (1986); 26: Nilsson et al. (2001a); 27: Nilsson et al. (2001b).

References

Alvarez, R., & Plez, B. 1998, A&A, 330, 1109
Alonso, A., Arribas, S., & Martínez-Roger, C. 1999, A&AS, 139, 335
Anders, E., & Grevesse, N. 1989, Geochim. Cosmochim. Acta, 53, 197
Andersen, T., Poulsen, O., & Ramanujam, P. S. 1975, Sol. Phys., 44, 257
Anstee, S. D., & O'Mara, B. J. 1995, MNRAS, 276, 859
Anthony-Twarog, B. J., & Twarog, B. 2000, AJ, 119, 2282
Aoki, W., Norris, J. E., Ryan, S. G., Beers, T. C., & Ando, H. 2000, ApJ, 536, L97
Arlandini, C., Käppeler, F., Wisshak, K., et al. 1999, ApJ, 525, 886
Asplund, M., & García Pérez, A. E. 2001, A&A, 372, 601
Asplund, M., Gustafsson, B., Kiselman, D., & Eriksson, K. 1997, A&A, 318, 521
Barbuy, B. 1988, A&A, 191, 121
Barklem, P. S., & O'Mara, B. J, 1997, MNRAS, 290, 102
Barklem, P. S., O'Mara, B. J., & Ross, J. E. 1998, MNRAS, 296, 1057
Bauschlicher, C. W., Langhoff, S. R., & Taylor, P. R. 1988, ApJ, 332, 531
Beers, T. C., Preston, G. W., & Schectman, S. A. 1992, AJ, 103, 1987

Beers, T. C. 1999, in Third Stromlo Symp.: The Galactic Halo, ed. B. Gibson, T. Axelrod, & M. Putman (San Francisco: ASP), 165, 206
Beers, T. C., Flynn, C., Rossi, S., et al. 2002a, in preparation
Beers, T. C., Rossi, S., Anthony-Twarog, B., et al. 2002b, in preparation
de Bernardis, P., Ade, P. A. R., Bock, J. J., et al. 2000, Nature, 404, 955
Bergström, H., Biémont, E., Lundberg, H., & Persson, A. 1988, A&A, 192, 335
Bessell, M., & Norris, J. 1984, ApJ, 285, 622
Biémont, E., Grevesse, N., Hannaford, P., & Lowe, R. M. 1981, ApJ, 248, 867
Biémont, E., & Youssef, N. H. 1984, A&A, 140, 177
Biemont, E., Grevesse, N., Hannaford, P., & Lowe, R. M. 1989, A&A, 222, 307
Biémont, E., & Lowe, R. M. 1993, A&A, 273, 665
Boesgaard, A. M., King, J. R., Deliyannis, C. P., & Vogt, S. S. 1999, AJ, 117, 492
Burbidge, G. R., & Burbidge, E. M. 1955, ApJS, 1, 431
Burstein, D., & Heiles, C. 1982, AJ, 87, 1165
Burris, D. L., Pilachowski, C. A., Armandroff, T. E., et al. 2000, ApJ, 544, 302
Cayrel, R. 1996, A&AR, 7, 217
Cayrel, R., Hill, V., Beers, T. C., et al. 2001, Nature, 409, 691
Cerny, D., Bacis, R., Guelachvili, G., & Roux, F. 1978, JMS, 73, 154
Colarusso , P., Lebeault-Dorget, M.-A., & Simard, B. 1997, Phys. Rev., 55, 1526
Corliss, C. H., & Bozman, W. R. 1962, Experimental Transition Probabilities for Spectral lines of Seventy Elements (NBS Monograph 32) (Washington: GPO)
Cowan, J. J., Pfeiffer, B., Kratz, K.-L., et al. 1999, ApJ, 521, 194
Cowley, R. C., Aikman, G. C. C., & Fisher, W. A. 1977, Publ. Dom. Astrophys. Obs. Victoria, 15, 37
Crawford, J. L., Sneden, C., King, J. R., Boesgaard, A. M., & Delyannis, C. 1998, AJ, 116, 2489
Cutri, R. M., Skrutskie, M. F., van Dyk, S., et al. 2000, Second Incremental Data Release Explanatory Supplement, `http://www.ipac.caltech.edu/2mass/releases/second/doc/explsup.html`
Dekker, H., D'Odorico, S., Kaufer, A., Delabre, B., & Kotzlowski, H. 2000, in Optical and IR Telescope Instrumentation and Detectors, ed. Masanori Iye and Alan F. Moorwood, Proc. SPIE 4008, 534
Depagne, E., et al. 2002, in preparation
Edvardsson, B., Andersen, J., Gustafsson, B., et al. 1993, A&A, 275, 101
Fouqué, P., Chevallier, L., Cohen, M., et al. 2000, A&AS, 141, 313
Gallagher, A. 1967, Phys. Rev., 157, 24
Goly, A., Kusz, J., Nguyen Quang, B., & Weniger, S. 1991, J. Quant. Spectrosc. Radiat. Transfer, 45, 157
Goriely, S., & Arnould, M. 2001, A&A, in press
Goriely, S., & Clerbaux, B. 1999, A&A, 346, 798
Gratton, R. G., & Sneden, C. 1994, A&A, 287, 927
Gustafsson, B., Bell, R. A., Eriksson, K., & Nordlund, Å. 1975, A&A, 42, 407
Gustafsson, B., & Mitzuno-Wiedner, M. 2001 in Astrophysical Timescales, PASP Conf. Ser., 245, 271
Hannaford, P., Lowe, R. M., Grevesse, N., Biémont, E., & Whaling, W. 1982, ApJ, 261, 736
Hill, V., Plez, B., Cayrel, C., & Beers, T. 2001 in Astrophysical Timescales, PASP Conf. Ser., 245, 316
Israelian, G., García López, R., Ramón, J., & Rebolo, R. 1998, ApJ, 507, 805
Ito, H., Ozaki, Y., Suzuki, K., Kondow, T., & Kuchitsu, K. 1988, JMS, 127, 283
Ivanova, D. V., & Shimanskii, V. V. 2000, Astr. Rep., 44, 376
Jaschek, M., & Malaroda, S. 1970, Nature, 225, 246
Johnson, J., & Bolte, M. 2001, ApJ, 554, 888
Jørgensen, U. G., Larsson, M., Iwamae, A., & Yu, B. 1996, A&A, 315, 204
Käppeler, F., Beer, H., & Wisshak, K. 1989, Rep. Prog. Phys., 52, 945
Kotlar, A. J., Field, R. W., & Steinfeld, J. I. 1980, JMS, 80, 86
Kupka, F., Piskunov, N. E., Ryabchikova, T. A., Stempels, H. C., & Weiss, W. W. 1999, A&AS, 138, 119
Kurucz, R. L. 1993, CD-rom, 15
Kusz, J. 1992, A&AS, 92, 517
Kwiatkowski, M., Zimmermann, P., Biémont, E., & Grevesse, N. 1984, A&A, 135, 59
Lage, C. S., & Whaling, W. 1976, J. Quant. Spectrosc. Radiat. Transfer, 16, 537
Larsson, M., Siegbahn, P. E. M., & Agren, H. 1983, ApJ, 272, 369
Lawler, J. E., Bonvallet, G., & Sneden, C. 2001a, ApJ, 556, 452
Lawler, J. E., Wickliffe, M. E., Sen Harog, E. A., & Sneden, C. 2001b, ApJ, 563, 1088
Lawler, J. E., Wickliffe, M. E., Cowley, C. R., & Sneden, C. 2001c, ApJS, 137, 341
Lu, L., Sargent, W. W., Barlow, T. A., Churchill, C. W., & Vogt, S. S. 1996, ApJS, 107, 475
Luque, J., & Crosley, D. R. 1999, SRI Int. Rep. MP 99-009
Maier, R. S., & Whaling, W. 1977, J. Quant. Spectrosc. Radiat. Transfer, 18, 501
McWilliam, A., Preston, G. W., Sneden, C., & Searle, L. 1995, AJ, 109, 2757
Meyer, D. M., & Roth, K. C. 1991, ApJ, 376, L49
Michaud, G., Charland, Y., Vauclair, S., & Vauclair, G. 1976, ApJ, 210, 447
Moore, C. E. 1970, Ionization potentials and Ionization Limits Derived from the Analyses of Optical Spectra, Natl. Bur Stand. (US) Circ. No. NSRDS-NBS 34 (U.S. GPO Washington D.C., 1970)
Musiol, K., & Labuz, S. 1993, Phys. Scr., 27, 422
Nilsson, H., Ivarsson, S., Johansson, S., & Lundberg, H. 2001, A&A, 381, 1090
Nilsson, H., Zhang, Z., Lundberg, H., Johansson, S., & Nordström, B. 2001, A&A, 382, 368
Nissen, P., Primas, F., & Asplund, M. 2001, New Astron. Rev., 45, 545
Norris, J. E., Ryan, S. G., & Beers, T. C. 2001, ApJ, 561, 1034
Pagel, B., & Tautvaišienè, G. 1997, MNRAS, 288, 108
Plez, B. 1998, A&A, 337, 495
Plez, B., Brett, J. M., & Nordlund, Å. 1992, A&A, 256, 551
Plez, B., Smith, V. V., & Lambert, D. L. 1993, ApJ, 418, 812
Prantzos, N., Hashimoto, M., & Nomoto, K. 1990, A&A, 234, 211
Prasad, C. V. V., & Bernath, P. F. 1992, JMS, 156, 327
Prasad, C. V. V., Bernath, P. F., Frum, C., & Engleman, R. Jr. 1992, JMS, 151, 459
Qian, Y.-Z., & Wasserburg, G. J. 2001a, 552, L55

Qian, Y.-Z., & Wasserburg, G. J. 2001b, 559, 925
Qian, Y.-Z., & Wasserburg, G. J. 2002, 567, 515
Reader, J., & Sansonetti, C. J. 1986, Phys. Rev., 33, 1440
Rehfuss, B. D., Suh, M. H., & Miller, T. A. 1992, JMS, 151, 437
Ryan, S. G., Norris, J. E., & Beers, T. C. 1992, ApJ, 471, 254
Schatz, H., Toejnes, R., Kratz, K.-L., et al. 2002, in preparation
Schlegel, D. J., Finkbeiner, D. P., & Davis, M. 1998, ApJ, 500, 525
Sneden, C., McWilliam, A., Preston, G. W., et al. 1996, ApJ, 467, 819
Sneden, C., Cowan, J. J., Burris, D. L., & Truran, J. W. 1998, ApJ, 496, 235
Sneden, C., Cowan, J. J., Ivans, I. I., et al. 2000a, ApJ, 533, L139
Sneden, C., Johnson, J., Kraft, R. P., et al. 2000b, ApJ, 536, L85
Sneden, C., & Primas, F. 2001, New Astron. Rev., 45, 545
Sneden, C., Cowan, J. J., Lawler, J. E., et al. 2002, ApJ, 556, L25
Spite, M. 1967, Ann. Astrophys., 30, 211
Tsujimoto, T., Shigeyama, T., & Yoshii, Y. 2000, ApJ, 531, L33
Umeda, H., & Nomoto, K. 2002, ApJ, 565, 385
Van Eck, S., Goriely, S., Jorissen, A., & Plez, B. 2001, Nature, 412, 793
Vladilo, G., Bonifacio, P., Centurión, M., & Molaro, P. 2000, ApJ, 543, 24
Ward, L., Vogel, O., Ahnesjö, A., et al. 1984, Phys. Scr., 29, 551
Ward, L., Vogel, O., Arnesan, A., Hallin, R., & Wännström, A. 1985, Phys. Scr., 31, 161
Westin, J., Sneden, C., Gustafsson, B., & Cowan, J. J. 2000, ApJ, 530, 783
Wickliffe, M. E., Salih, A., & Lawler, J. E. 1994, JQSRT, 51, 545
Wisshak, K., Voss, F., & Käppeler, F. 1996, in Proc. 8th Workshop on Nuclear Astrophysics, ed. W. Hillebrandt, & E. Müller (Munich, MPI), 16